Swarming midges as self-propelled particles with long-range interactions

Thesis submitted to
Indian Institute of Science Education and Research Pune
towards the partial fulfilment of BS-MS dual degree programme
by

RAGHAV SHARMA

27 MARCH 2024

under the guidance of

Supervisor: PROF. NIR GOV

Co-supervisor: DR. DAN GORBONOS

from May 2023 to March 2024

Certificate

This is to certify that this dissertation entitled **Swarming midges as self-propelled particles with long-range interactions** towards the partial fulfilment of the BS-MS dual degree programme at the Indian Institute of Science Education and Research, Pune, represents work carried out by Raghav Sharma at the Indian Institute of Science Education and Research, Pune, under the supervision of Prof. Nir Gov, Department of Chemical and Biological Physics, Weizmann Institute of Science, Israel, and under the co-supervision of Dr. Dan Gorbonos, Department of Collective Behaviour, Max Planck Institute of Animal Behavior, Germany, during the academic year 2023-2024.

Dan Gorbonos

Nir Gov

Committee:

Prof. Nir Gov

Dr. Dan Gorbonos

Prof. Vijayakumar Chikkadi

Declaration

I hereby declare that the matter embodied in the report entitled **Swarming midges as self-propelled particles with long-range interactions** are the results of the work carried out by me at the Department of Chemical and Biological Physics, Weizmann Institute of Science, Israel, under the supervision of Prof. Nir Gov, Department of Chemical and Biological Physics, Weizmann Institute of Science, Israel and under the co-supervision of Dr. Dan Gorbonos, Department of Collective Behaviour, Max Planck Institute of Animal Behavior, Germany, and the same has not been submitted elsewhere for any other degree. Wherever others contribute, every effort is made to indicate this clearly, with due reference to the literature and acknowledgment of collaborative research and discussions.

Raghav Sharma
Roll no.: 20191087
Date: 27 March 2024

ACKNOWLEDGMENTS

Firstly, I would like to express my deepest gratitude to my supervisors, Prof. Nir Gov and Dr. Dan Gorbonos, for their unwavering support, guidance, and mentorship throughout this journey. The discussions we had, their insights, and feedback were invaluable in shaping my approach to research. Their expertise in the applications of physics and ability to translate complex concepts with clarity have been pivotal in challenging and expanding my understanding of the subject. They have provided me with an environment where questioning and curiosity were welcomed. This freedom to explore has been a cornerstone of time here.

I am profoundly grateful to all the members of the Nir Gov Lab, especially Dr. Shubhadeep, for their collaboration, camaraderie, and the stimulating discussions we shared. Their expertise and willingness to give their time so generously were very much appreciated. I want to extend my sincere appreciation to Sameernandan for sharing their lab space with me and for insights that significantly enriched my research experience. Additionally, I am thankful for the lessons in quantum physics and chemistry. These friendships and intellectual companionship have been a cornerstone of my research journey. They have been a constant source of inspiration.

Special thanks to the member of my TAC, Prof. Vijayakumar Chikkadi, for his continued support. Prof. Chikkadi's great, well-rounded course on Soft Matter introduced concepts that I could apply to the swarming system. He was always available when I needed advice.

I am also grateful to my family members, especially my grandmother, parents, Deepanshi, Swati, Sajal, Suhali, Chirayu, Aditya and the esteemed members of LDAB for their love and sacrifices. Madhu and Soham, my fellow Michael Kern apartment mates, are great friends who have made my time in Israel the most memorable. Each and every one of them is part of my life that makes it greater than the sum of its parts. I appreciate their encouragement and the light-hearted moments that sustained me through challenging times.

I want to thank the administrative staff at the Weizmann Institute for their assistance and help throughout my time in Israel.

Lastly, and most importantly, I would like to thank Chironomus midges for swarming. They are the catalysts that made the aforementioned possible.

Contents

LIST OF FIGURES

LIST OF TABLES

ABSTRACT

In this thesis, we explore the complex dynamics of swarming midges through the lens of the adaptive gravity model, enhanced to include self-propulsion and noise. This study is motivated by the observation that midges, engage in the collective behaviors of swarming, which are disordered self-organization structures. Through molecular dynamics simulations, we demonstrate that our modified model—adaptive gravity model for self-propelled particles—not only reproduces the cohesive behavior observed in natural midge swarms but also elucidates many of their complex dynamical properties. This work contributes to the broader understanding of collective behaviors in biological systems, presenting a novel active matter model that bridges the gap between biological interactions and the emergent complexity of natural swarms.

Chapter 1

INTRODUCTION

Organisms commonly form aggregates that exhibit emergent collective behavior, with group dynamics distinct from individuals' behavior. Such collective behavior encompasses the fascinating phenomena of flocking and swarming, prime examples of how individual organisms can coordinate their actions to produce complex, large-scale patterns and movements. Flocking, often observed in birds such as starlings, involves a highly synchronized and cohesive movement where individuals align their velocity and direction[1]. This behavior is not only mesmerizing to watch but also serves practical purposes, such as predator evasion and increased foraging efficiency[2]. Flocks are characterized by the individual particles breaking rotational symmetry, which results in a global, polarized structure. While flocks are characterized by order, swarms, on the other hand, are inherently disordered.

Swarming can be seen in insects where individuals move more loosely than flocking, often forming a cloud-like formation that can expand, contract, and shift direction fluidly. Many species within the extensive taxonomic order Diptera, which includes flies, mosquitoes, and midges, create large swarms primarily composed of males, with the primary goal of attracting females[3]. Thus, swarming plays a crucial role in reproduction. In this study, our insect of focus is the non-biting midge *Chironomus riparius*. The male midge has a body length of approximately 7 mm. Male midges typically fly at speeds around 0.5 ms^{-1}, with peak accelerations reaching about 5 ms^{-2}[4]. During their adult phase, male midges autonomously gather in mating swarms, called leks, twice a day, at sunrise and sunset, above a designated swarm marker. It is important to highlight that each

swarm initially comprises only a small group of airborne males. More males may gradually join the swarm, and the average number of participating individuals may take a few minutes to stabilize. Female individuals do not engage in swarming behavior; however, they may fly through the swarms in search of mates– swarms are a way for the males to collectively attract the females[5][6]. Additionally, these swarms are stationary and possess no net velocity ordering. Despite a lack of global order, swarm particles are tightly bound to the swarm and exhibit long-range correlations within the swarm[7]. It is known that the swarms form in the presence of a marker, such as a light source or surface of water. This does seem to explain why particles are bound to the swarm but not the correlations. Furthermore, some studies posit that the correlation is weak; however, these studies, too, make a case that swarming is a collective behavior as the outer boundary of the swarm is quite sharp, in a statistical sense, and does not line up with the boundary of the swarm marker[8]. Thus, swarms pose an interesting problem: an emergent coherent structure that appears disconnected.

Researchers use theoretical modeling to make sense of the empirical data from collectively behaving biological systems[9]. Due to the complexity of such systems, it is perhaps more productive to think of models of collective behavior not as generic, holistic descriptions of the system but as tools to understand specific aspects of how collective behavior functions[10]. Modeling emergent behaviors like the collective behaviors mentioned above requires two main components- individual behaviors and interaction rules[11]. Modeling these behaviors using simple interaction rules has had great success in reproducing complex collective behaviors[12]. Modeling helps reduce complex behavior to understandable and quantifiable rules. Today, it is a well-accepted idea in biology that aggregations of individuals subject only to local behavioral rules can self-organize into complex coherent groups, as in physical systems[13]. The units that make up biological systems possess a level of complexity far beyond that of the inanimate particles found in physical systems, with capabilities for cognition and variation across different species. Although it might seem logical to assume that this individual complexity is superfluous mainly, with only a handful of traits necessary to understand the formation of groups, there is no predefined way to determine which aspects are pertinent and which are not. This determination often hinges on the specific nature of the inquiry and the observational scale of the collective behavior in question. Therefore, the

challenge of identifying relevant details is significant, and at certain points, the attributes of the individual play a central role[10]. Determining the traits to include or, equivalently, the essential characteristics to attribute to the particles in your model constitutes the essence of modeling collective animal behavior. Specifically, in agent-based models, one must define the default, solitary behavior of each entity; select a mathematical model for the interactions that link these entities; ascertain if these interaction rules are consistent across the population and over time; and identify which entities will interact with each other[4].

Modeling also provides additional advantages in addition to reproducing collective behaviors. These models enable researchers to systematically explore the effects of varying parameters (such as the number of individuals, the strength of their interactions, and environmental influences) on collective behavior. This exploration can uncover the conditions under which specific behaviors emerge, persist, or collapse, shedding light on the stability and adaptability of these systems. Beyond theoretical understanding, collective behavior models can inform real-world applications, such as the design of algorithms for autonomous robotic swarms[14].

Models that elucidate collective behavior generally fall into one of two categories: continuum models and agent-based models. The fundamental concept of continuum modeling revolves around characterizing the system through variables such as density, velocity, and other large-scale fields that change over space and time. Rather than concentrating on the actions of individual entities, continuum models employ partial differential equations to capture the progression of these macroscopic fields. The principles of fluid dynamics greatly influence this methodology, employing analogous equations to articulate how fluids and gases move and behave[15][10]. In contrast to continuum models that represent systems as uniform and continuous fields, agent-based models focus on simulating each agent individually. This approach enables the investigation of intricate behaviors and patterns that arise organically from the ground up. Therefore, rather than relying on a singular partial differential equation (PDE) system, an agent-based model comprises a series of coupled ordinary differential equations (ODEs). Continuum modeling proves especially advantageous for managing scenarios involving large numbers of entities, such as bird flocks, fish schools, or bacterial colonies. On the other hand, agent-based models are better suited for smaller or sparser groupings. In essence, agent-based models represent the most fundamental approach to character-

izing a gathering of animals. A continuum model, by nature, simplifies what is a discrete system; furthermore, through the application of coarse-graining techniques from statistical mechanics, one can always generate a continuum model starting from an agent-based model. Furthermore, an agent-based model allows for the detailed depiction of each individual's dynamics, incorporating variations and changes over time at the population level. Consequently, agent-based models offer greater versatility, capturing a broader array of behaviors compared to more generalized models. In this thesis, the focus will be on discussing agent-based modeling of swarming midges.

Chironomid midges are highly responsive to sound and are believed to be drawn toward swarms by the noise generated within. The sound emanating from the beating wings of a male midge covers a wide range of frequencies, yet it prominently features a fundamental frequency of around 575 Hz. Inspired by such findings, Gorbonos et al.[4][16][17][18] propose and show through their adaptive gravity model that swarming midges are drawn towards the sounds emitted by their counterparts and this acoustic communication underlies the large-scale collective behavior of the swarm. The sound field generated by airborne insects includes a monopole element, the strength of which diminishes following an inverse square law, mirroring the decrease of gravitational force with increasing separation between objects. Components of the sound field with dipole and higher orders decay faster, making them less potent than the monopole element. The model introduces an innovative concept by exploiting the similarity in form between the decay of acoustic and gravitational forces, thereby formulating a gravity-like model that allows borrowing its established computational and analytical tools. Additionally, central to their model is the concept of adaptivity in the acoustic interactions among midges within a swarm. Adaptivity is the property of animals to respond to the relative fold-change in a signal that reaches its sensory organs[19]. Adaptivity in this context refers to the midges' capacity to adjust their response to acoustic signals based on their environment's overall sound intensity. Essentially, when the intensity of sound escalates—suggesting a greater concentration of midges nearby—each midge adjusts by altering its responsiveness to these acoustic stimuli. This adaptive response ensures that each midge's reaction to the swarm's collective sound is scaled appropriately, preventing overstimulation and enabling the swarm to maintain its coherence without centralized control. This leads to an emergent, collective behavior that closely mirrors the self-organized patterns observed in nature, including creating

and maintaining swarms without the need for external limits or specific guidelines defining the swarm. Since the swarms are such stochastic structures, different modeling approaches can create natural-looking swarm-like structures. Additionally, since global order or strong long-range correlations are neither necessary nor sufficient conditions to characterize a swarm[8], the authors looked at different physical measurements of the swarms to validate the modeling scheme. The adaptive gravity model successfully captured critical features of swarm dynamics, including effective spring constants that vary with swarm size, the non-Gaussian distribution of accelerations and velocities, and the vertical elongation of enormous swarms[4]. Furthermore, the authors independently compared the effects of long-range attraction and long-range attraction with adaptivity. This was done using analytical and numerical Newtonian gravity results (long-range attraction only) and numerical adaptive gravity results (long-range attraction with adaptivity)[17]. Some results, like negative scaling of density at the center of the swarm with swarm size, corroborate with Newtonian gravity; however, other results, such as the uniform average speed with distance, could only be produced by adaptive gravity. Hence, the adaptive gravity model offers a solid foundation for examining how complex collective behaviors emerge from long-range interactions modulated by sensory adaptation.

For all the success of the adaptive gravity model, its significant flaws lie in the framework's assumption. Biological entities are not like passive particles that are subject to Newtonian gravity. Furthermore, biological systems are inherently noisy–with both external and internal sources. Therefore, we take the adaptive gravity model forward and add self-propulsion and noise to create a more realistic description. These modifications are hereafter referred to as the adaptive gravity model for self-propelled particles. These modifications alter the modeling equations (section 2.2). We run molecular dynamics simulations to emulate natural swarms. The adaptive gravity model for self-propelled particles successfully reproduces all the success of the adaptive gravity model and some with a stronger trend(chapter 3), such as scaling of numbers with swarm size, etc. Additionally, it gives noise as a free parameter that can be used to change the dynamics of the swarm (section 3.3).

In this thesis, we introduce a model that exhibits emergent self-organizing dynamics, featuring

self-propelled particles with long-range interactions scaled by a function that depends on the system's geometry.

Chapter 2

MODEL

2.1 ADAPTIVE GRAVITY MODEL

The model is called the adaptive gravity model and can be thought of as akin to many body simulations done for astrophysical objects. In this model, simulation particles (which represent individual insects) can be thought of as planets or stars interacting through a gravitational potential, albeit modified, following r^{-2} dependence.

The sound produced by a flying insect originates from the movement of its wings, creating a sound field that includes both monopole and dipole elements. Given that the monopole component decays at a slower rate than the dipole component, our attention will be primarily on the monopole aspect. Midges detect sound via the deflection of hairs on their antennae, which is induced by the sound waves that pass by. This detection mechanism necessitates that the sound waves apply a force to these hairs. Consequently, it's essential to investigate how the energy flow diminishes to understand the reduction of a sound signal emanating from an individual midge with increasing distance. In the case of a monopole source, the average flow decreases as r^{-2}, where r is the distance from the emitting midge.

The authors extend this assumption further by proposing that a single midge moves closer to a nearby midge by means of an effective force that is directly correlated with the intensity of sound. This implies that the force between two midges i and j separated by a distance r_{ij} will depend on r_{ij}^{-2}, similar to the gravitational pull experienced between two point masses. This is the simplest

assumption to make, given the limited experimental evidence. Indirect support for this assumption comes from the observation of a linear restoring force pulling towards the center of the swarm(see Figure 3.5 and Figure B.1). The pairwise interactions that could lead to a linear restoring force directed towards the center of the swarm is one that adheres to an inverse-square law. This forms the "gravity" part of the adaptive gravity model. According to this, the total force experienced by particle i due to particle j, $\vec{F}_{ij}$ is:

$$\vec{F}_{ij} = C\hat{r}_{ij}\frac{1}{r_{ij}^2} \tag{2.1}$$

Here, $\vec{r}_i$ is the position of midge i and; $\vec{r}_{ij} = \vec{r}_j - \vec{r}_i$ and; $r_{ij} = |\vec{r}_{ij}|$ and; $\hat{r}_{ij} = \vec{r}_{ij}/r_{ij}$; and C is constant akin to G for Newtonian gravity and has dimensions $M^1L^3T^{-2}$.

Additionally, the authors introduce the assumption that the acoustic perception of midges adjusts based on the overall sound intensity, and this response to sound varies with respect to a length scale R_{ad}. This assumption is based on the understanding that biological systems have the capability to regulate signal-to-noise ratio. This contributes to the "adaptive" part of the adaptive gravity model. The authors assume adaptivity to follow the fold-change detection mechanism. The fold-change detection refers to a system's ability to respond to relative changes in input signal strength, such as the fold increase or decrease in concentration of a signaling molecule, rather than its absolute concentration. With this addition, the effective force between two midges $\vec{F}_{ij}$ is :

$$\vec{F}_{ij} = C\hat{r}_{ij}\frac{1}{r_{ij}^2}\frac{R_{\text{ad}}^{-2}}{\sum_{k\neq i}^{N} r_{ik}^{-2} + R_{\text{ad}}^{-2}} \tag{2.2}$$

Here, R_{ad} is the aforementioned length scale for adaptivity. When a single midge is closer than R_{ad}, the sound it emits is strong enough that the receiving midge needs to adapt its sensitivity, thereby diminishing the intensity of the perceived signal. Beyond this distance, there is no need for such adaptivity for the sound of a single midge.

For simulation, we kept $C = 1$, and we omitted this in further equations.

The normalization factor in the adaptive gravity force, f_{ad}, can be represented as:

$$f_{\text{ad}}(r_i) = \frac{R_{\text{ad}}^{-2}}{\sum_{k\neq i}^{N} r_{ik}^{-2} + R_{\text{ad}}^{-2}} = \frac{1}{1 + \sum_{k\neq i}^{N} (R_{\text{ad}} r_{ik}^{-1})^2} \tag{2.3}$$

This could be compared with another function that represents fold change detection– Hill function:

$$g_{\text{Hill}}(x) = \frac{1}{1 + (Kx^{-1})^n} \tag{2.4}$$

Here, K is similarly a characteristic scale for x; and n, called the Hill coefficient, is a sensitivity parameter. The Hill function is widely used in biochemistry and systems biology to describe how a system's output response depends on the concentration of an input signal, often in the context of enzyme kinetics, gene regulation, and signal transduction pathways. In the context of fold-change detection, the Hill coefficient n plays a crucial role. A higher n value indicates a more cooperative system, where the response is more sensitive to changes in the stimulus concentration. This cooperativity can contribute to a system's ability to detect fold changes in the input signal because it makes the response function steeper, allowing for a more pronounced response to relative changes in signal concentration. We can draw similar parallels for adaptive gravity. When other particle distances are closer than R_{ad}, the force is normalized by a smaller factor than when the distances are farther away than R_{ad}.

A notable characteristic of this force is that it diverges from the principle of superposition observed in Newtonian gravity, as the force experienced at each point is influenced not just by the distance and position of surrounding bodies but also by the particle's position. Consequently, in this framework, each midge experiences a force that conveys global, long-range information about the swarm. Yet, this force does not allow for the identification of the influence exerted by any neighbor. Thus, in this model, the force that links individual midges to the swarm emerges as a collective, group-level phenomenon, naturally arising from the swarm itself without reliance on external factors. Moreover, traditional conservation laws, such as those for momentum or energy, do not apply in this context, except for the conservation of mass or number. As a result, the total sum of forces does not equal zero, leading to the acceleration of the swarm's center of mass. Nevertheless, this does not affect the internal dynamics of the swarm. All the calculations shown in chapter 3 are taken by making the acceleration and velocity of the swarm center zero.

It's important to recognize that in the absence of an extra mechanism, like self-propulsion or

a short-range repulsive force, a purely attractive interaction, as depicted in our adaptive gravity model, might lead to collapse. For the purpose of analytical computations, the authors proceed under the assumption of swarms with uniform density, suggesting the implicit presence of a mechanism to prevent collapse. In their model simulations, they introduce a short-range repulsive force inspired by empirical evidence. Moving forward with this research, we adopt a comparable assumption and methodology.

2.2 ADAPTIVE GRAVITY MODEL FOR SELF-PROPELLED PARTICLES

To recapitulate, the foundational assumptions of the adaptive gravity model are that midges communicate and react based on the intensity of sound, and they adjust their sensitivity to this sound intensity. Building on the existing framework, we introduce three additional assumptions. The adaptive gravity model originally conceptualized insect individuals as non-living entities akin to planets without any inherent directional movement. We modify these parameters and infuse our model with "vitality".

In our refined approach, insects are conceptualized as self-propelled active particles, each characterized by a unique heading direction and a velocity relaxation time. The notion of self-propulsion suggests that, without external influences, a particle would maintain a constant speed, denoted as v_0, and consequently execute an unbiased random walk. Unlike the adaptive gravity model, where forces directly influence acceleration, our enhancement posits that forces now primarily serve to alter the particle's heading direction, represented as $\vec{n}$. Although the heading direction adjusts instantaneously in response to force, it constitutes only a component of the particle's acceleration. Moreover, we incorporate a velocity relaxation time, τ_v, into our model, acknowledging that biological entities cannot change their velocity directions instantaneously. With these modifications, our modeling scheme has changed drastically. We begin by describing our acceleration for particle i:

$$\frac{d\vec{v}_i}{dt} = -\beta(\vec{v}_i - v_0\hat{n}_i) + \vec{\varepsilon}_i \tag{2.5}$$

Here, $\vec{v}_i$ is the velocity of particle i; v_0 is the self-propulsion speed; $\hat{n}_i$ is the unit vector of heading direction $\vec{n}_i$ of particle i; $\beta = \tau_v^{-1}$ is the inverse relaxation time; and $\vec{\varepsilon}_i$ is a vector representing noise, sampled from a sphere of radius $\varepsilon/2$ centered at 0.

Let's ignore $\vec{\varepsilon}$, and any external force to rewrite the equation.

$$\frac{d\vec{v}}{dt} = -\beta(\vec{v} - v_0\hat{n}) \tag{2.6}$$

In the absence of any external influence or zero force, $\hat{n}$ becomes a constant. This will eventually make the acceleration zero as it is– $\frac{dv'}{dt} = -v'$ making $\vec{v} = v_0\hat{n}$. This is what makes v_0 the self-propulsion speed. Adding $\vec{\varepsilon}$ back to the above equation makes the particle do a random walk.

Again, ignoring $\vec{\varepsilon}$, we focus on our equation. However, now that $\hat{n}$ is not fixed here, we focus on making relaxation time $\tau_v \equiv \beta^{-1} \to 0$.

$$\beta^{-1}\frac{d\vec{v}}{dt} = -(\vec{v} - v_0\hat{n}) \tag{2.7}$$

As relaxation time goes to zero, we get $\vec{v} = v_0\hat{n}$. As the heading direction and, thereby, its unit vector $\hat{n}$ changes, the velocity also adapts to it instantaneously. This does not happen for biological systems justifying our need for a relaxation time.

Now, we discuss the heading direction. As mentioned earlier, the heading direction is equivalent to forces. Heading direction can be further expanded as a contribution of three forces- inter-particle adaptive gravitation $\vec{F}_{\text{adaptive},i}$, inter-particle short-range repulsion $\vec{F}_{\text{repulsion},i}$, and a short-range confinement potential to keep the swarm bounded within the simulation arena $\vec{F}_{\text{marker},i}$. Heading direction $\vec{n}_i$ for i^{th}-particle is:

$$\vec{n}_i = \underbrace{\left[\sum_{j\neq i}^{N} \hat{r}_{ij}\frac{1}{r_{ij}^2+\alpha^2}\frac{1}{\sum_{k\neq i}^{N}\frac{R_{\text{ad}}^2}{r_{ik}^2+\alpha^2}+1}\right]}_{\vec{F}_{\text{adaptive},i}} + \underbrace{\left[\sum_{j\neq i}^{N}\vec{r}_{ij}\left(\frac{R_{\text{rep}}}{r_{ij}}\right)^{12}\right]}_{\vec{F}_{\text{repulsion},i}} + \underbrace{\left[-\hat{r}_i\frac{12}{R_{\text{marker}}}\left(\frac{r_i}{R_{\text{marker}}}\right)^{11}\right]}_{\vec{F}_{\text{marker},i}} \tag{2.8}$$

Here, N is the number of midges in the swarm; R_{rep} is the radius of a midge; and R_{marker} is the radius of the simulation arena. The adaptive force in equation 2.2 seems different than equation

2.8 for the additional factor α. The role of α is to prevent energy differences from midges coming too close. This is what $\vec{F}_{\text{repulsion},i}$ does too. α ensures that both $\vec{F}_{\text{adaptive},i}$ and $\vec{F}_{\text{repulsion},i}$ both don't start blowing up together, and the particles do not come very close and perform related slingshots, which might break up the swarm.

It's important to recognize that our model is based on simple assumptions that have the potential for increased complexity. Currently, in our model interactions, that are interpreted as "effective" forces, only influence the heading direction. However, in a more complex model interactions could affect v_0, which might also not be constant then. Further complexity could be introduced by associating a relaxation time with the heading direction, which would give us an equation equivalent to Equation 2.5 but for $\hat{n}$.

2.3 METHODS

The numerical approach employed herein is an agent-based molecular dynamics simulation of particles. While a myriad of agent-based models exist to examine collective behavior, they all possess some common features. The quintessential element of an agent-based model is the individual agent, typically representing an individual animal, making the model distinct through the specific behavioral attributes assigned to each agent. Fundamentally, an agent-based model necessitates the definition of how an individual behaves autonomously, its criteria for selecting other agents for interaction, and the rules governing these interactions. The specifics of these elements for our model are highlighted in the preceding section.

2.3.1 INITIALIZATION

At the start of the simulation, particles are randomly distributed within a sphere centered around the origin, with a radius denoted as R_{init}. This initial distribution zone constitutes a relatively minuscule portion of the entire simulation domain—approximately $0.1R_{\text{marker}}$ linear size, equating to roughly one-thousandth of the total simulation area. Nonetheless, it exceeds the particle size, with $R_{\text{init}} \approx 10R_{\text{rep}}$, implying that the initial setup spans a volume about a hundred times greater than that of an individual particle. Therefore, during initialization, particles are significantly spaced

apart (Figure 3.1). Additionally, we implement a constraint that $v_0\Delta t < 2R_{\text{rep}}$ to prevent particles from approaching each other too closely within a single timestep before repulsive forces become effective.

Particles are initialized with a random velocity vector with magnitude v_0. We can even initialize particles with zeros velocity. So, as the simulation starts, the particle has $\vec{v} = 0$. Their acceleration is:

$$\frac{d\vec{v}}{dt} = \beta v_0 \hat{n} + \vec{\varepsilon} \tag{2.9}$$

Initially, particles behave similarly to the passive entities in simulations based on the adaptive gravity model, with their acceleration being determined by the effective force of mutual attraction. However, after several timesteps, this influence diminishes, resulting in the emergence of active, polarized particles endowed with associated viscosity.

In this part of the simulation, we also generate the noise vector $\vec{\varepsilon}$, which is uniformly sampled throughout the simulation. Three components of the noise vector were generated by taking three random numbers independently from a uniform distribution $\text{U}[-\frac{\varepsilon}{2}, \frac{\varepsilon}{2}]$. If the magnitude of this vector is less than $\varepsilon/2$, where ε is our external parameter for noise, then it is accepted otherwise rejected.

2.3.2 Time Evolution

We discretize our main equation (2.5), which will give us the change in velocity at each time step as follows:

$$\Delta\vec{v}_i = \frac{d\vec{v}_i}{dt}\Delta t = \beta\Delta t(-\vec{v}_i + v_0\hat{n}_i) + \vec{\varepsilon}_i\Delta t \tag{2.10}$$

Our system resembles a typical molecular dynamics system, wherein the forces or accelerations that update the velocities are contingent upon the system's configuration, namely the positions of the particles, and concurrently, the mechanism that updates the positions is dependent on the velocities, thereby establishing a set of coupled equations.

$$\vec{r}_{t+1,i} = \vec{r}_{t,i} + \vec{v}_{t,i}\Delta t \tag{2.11}$$

$$\vec{v}_{t+1,i} = \vec{v}_{t,i} + \left[\beta(v_0\hat{n}_{t,i} - \vec{v}_{t,i}) + \vec{\varepsilon}_{t,i}\right]\Delta t \tag{2.12}$$

Parameter description	Symbol	Typical values
Number of particles	N	$10 - 10^2$
Self-propulsion speed	v_0	$10 - 10^2$
Noise	ε	$10 - 10^2$
Inverse Relaxation time	β	$10^{-1} - 10^1$
Size of a particle	R_{rep}	1
Radius of adaptivity	R_{ad}	$10 - 10^2$
Size of initialization sphere	R_{init}	10^2
Size of simulation sphere	R_{marker}	10^3
Simulation time-step	Δt	10^{-2}
Total time	-	10^3
Prevent slingshot	α^2	$1 - 10$

Table 2.1: Typical parameter values used in the simulation that give a cohesive swarm

Here, the subscript t describes the physical quantity at timestep t.

To ensure precision, we employ the fourth-order Runge–Kutta integration method.

2.3.3 PARAMETERS

Typical parameter values used for performing simulations are shown in Table 2.1.

Chapter 3

RESULTS

In the previous section, we talked about our modeling scheme to capture the characteristic aspects of natural swarms. In this section, we compare the characteristic aspects of the natural swarms and compare them with natural swarms and adaptive gravity simulations to validate our model.

3.1 SWARMS

Firstly, we show that we get a stable swarm formation. We define the radius of the swarm R_S as the average distance of particles from the center of the swarm.

$$R_S(t) = \frac{1}{N}\sum_{i=1}^{N} |\vec{r}_i(t) - \vec{r}_{com}(t)| \tag{3.1}$$

Here, $\vec{r}_i$ is the position of i^{th}-particle and $\vec{r}_{com}$ is:

$$\vec{r}_{com}(t) = \frac{1}{N}\sum_{i=1}^{N} \vec{r}_i(t) \tag{3.2}$$

During the initialization, particles are randomly spread in a sphere of radius $R_{\text{init}} \sim 0.1R_{\text{marker}}$ without any velocity. As the system evolves in time, particles attract one another and start forming a swarm with small fluctuations about a constant radius R_S. This is what we refer to as a stable swarm. This behavior is seen in the Figure 3.1. The swarm radius is normalized by the radius

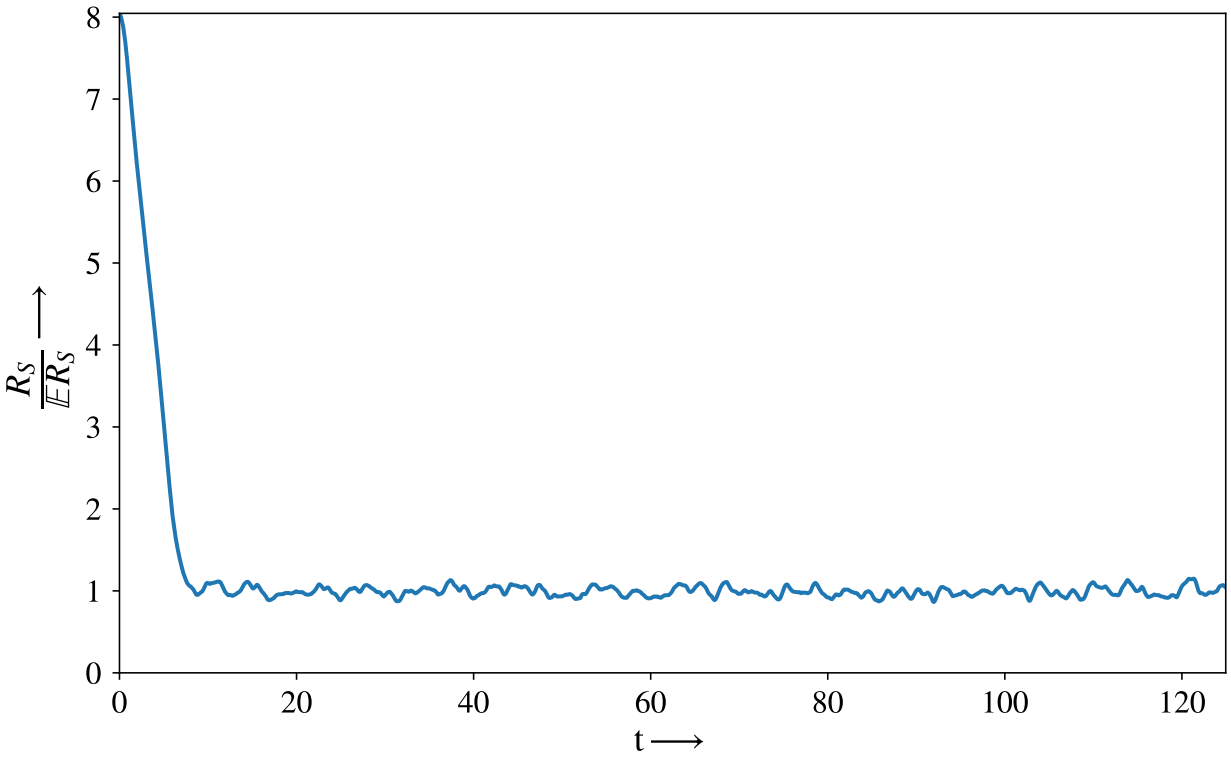

Figure 3.1: The size of the swarm R_S (normalized by its time-averaged value $\mathbb{E}[R_S]$) as a function of simulation time for a swarm with $R_{\text{ad}} = 10$ and $N = 55$. The swarm is stable for the duration of the simulation.

swarm averaged over time- $\mathbb{E}[R_S]$.

$$\mathbb{E}[R_S] = \frac{1}{\sum t} \sum R_S(t) \tag{3.3}$$

In the later part of the thesis, I will refer to $\mathbb{E}[R_S]$ by R_S, so it should be understood that it is a long-term average.

Additionally, the average kinetic energy of the swarm T_{swarm} follows a similar fashion. See figure Figure 3.2. At initialization, there is zero velocity and zero average kinetic energy. Just after initialization, particles accelerate toward the center of the swarm. Once they settle into a stable configuration, the mean kinetic energy fluctuates about a constant value.

$$T_{\text{swarm}} = \frac{1}{N} \sum_{i=1}^{N} \frac{|\vec{v}_i|^2}{2} \tag{3.4}$$

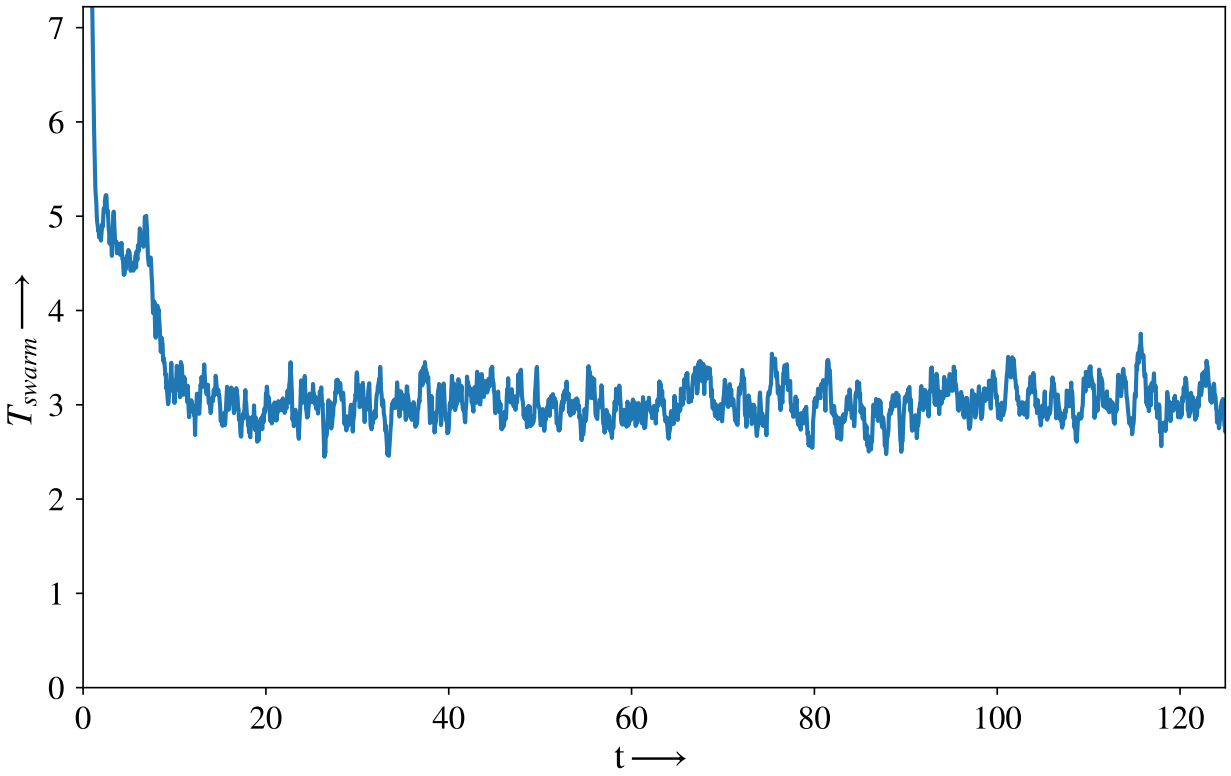

Figure 3.2: The mean kinetic energy of the swarm T_{swarm} as a function of simulation time for a swarm with $R_{\text{ad}} = 10$ and $N = 55$. The swarm kinetic energy is stable for the duration of the simulation.

We also show a random snapshot of the swarm in 3D in Figure 3.3.

After the system settles into a stable configuration, we wait for (about) ten times $v_0/2R_S$, or the time it takes for a particle to travel the diameter of the swarm, to start calculating statistics. In the program, the region of stable configuration is found using multiple least-squares algorithm, through which we identify multiple linear regions in Figure 3.1. After finding all the linear regions, the last such region is where the system has settled into a stable configuration.

3.2 STATISTICS

In previous papers on swarming[4][17] in midges, various quantities are mentioned and compared. The adaptive gravity model successfully reproduces and explains most of those metrics. With the adaptive gravity model for self-propelled particles, we wanted to observe its prowess since its

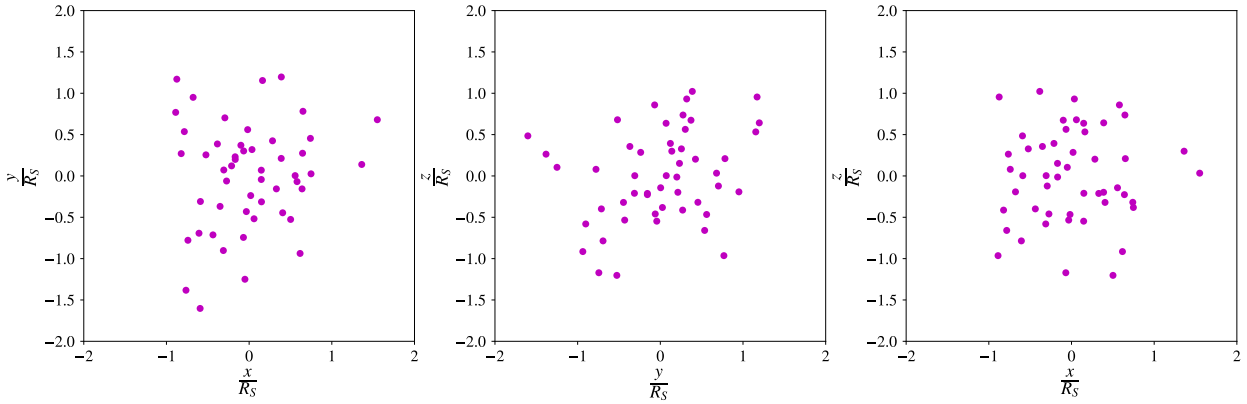

Figure 3.3: A random snapshot of a sample swarm for $N = 55$ is shown in three planes normalized by the R_S– $x-y$, $y-z$, and $x-z$. Particles are spread evenly about the center of the swarm.

underlying equations are different, i.e., force and acceleration are not directly related. We were impressed that most of the original relations were realized and that some were explained better than those with the adaptive gravity model. This section consists of many physical quantities that were compared. These quantities relate to the structure of the swarm.

3.2.1 Acceleration vs Position

An exciting observation found in the natural swarms is that near the center of the swarm(see Figure B.1), midges behave like simple harmonic oscillators- their acceleration was directly proportional to the distance from the center and its direction towards the center, i.e., $\ddot{x} \propto -x$. This property keeps the swarm a bounded structure, and it emerges in the simulations(Figure 3.5) without being explicitly coded into the equations. This is in contrast to [7], who impose a harmonic potential to keep the swarm bounded.

Figure 3.5 is generated by doing ten different runs, calculating each run's acceleration vs position profile, and averaging the results over all the runs. Then, we perform a least-squares fit against a function of the form $a_x = -\kappa_x * x : x \in [-0.25R_S, 0.25R_S]$. We do a similar analysis for the y-axis and z-axis (Figure 3.7).

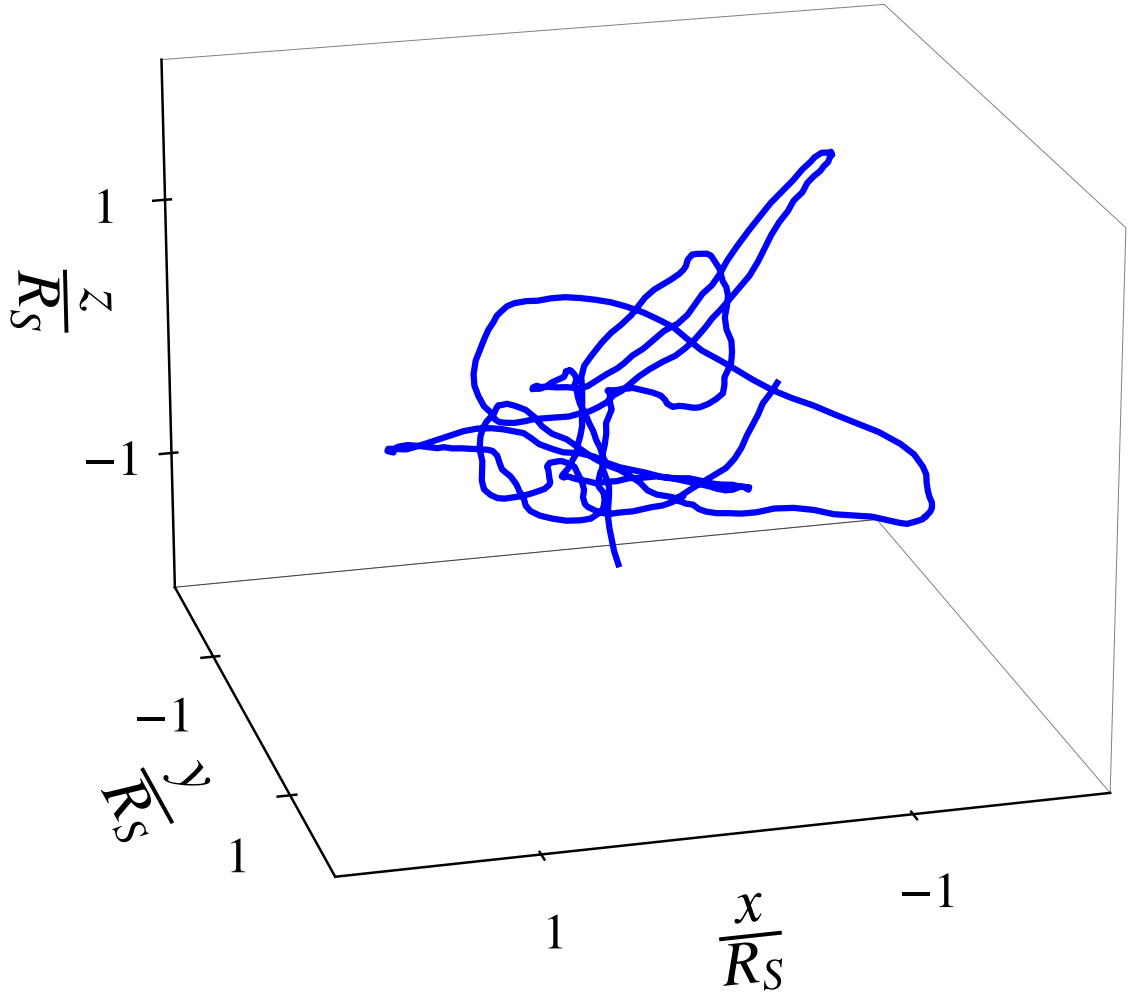

Figure 3.4: A random snapshot of a sample swarm trajectory for $N = 55$ is shown in three planes normalized by the R_S. For comparison with natural swarms, see Figure B.1.

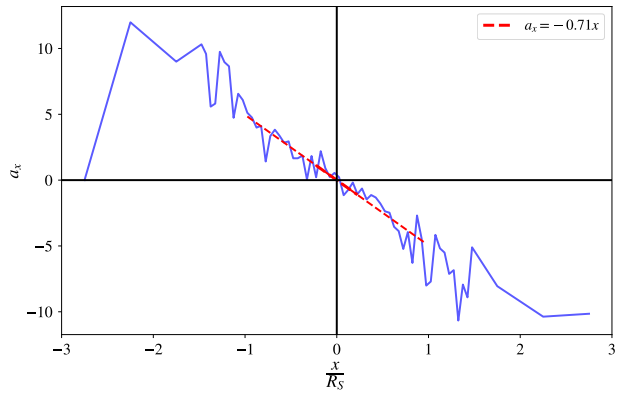

Figure 3.5: Mean value of x-component of acceleration as a function of x away from the center of the swarm. Note that about the center of the swarm, acceleration is linearly related with the position. The red dashed line shows a linear fit, and the calculated spring constant is shown in the top right box.

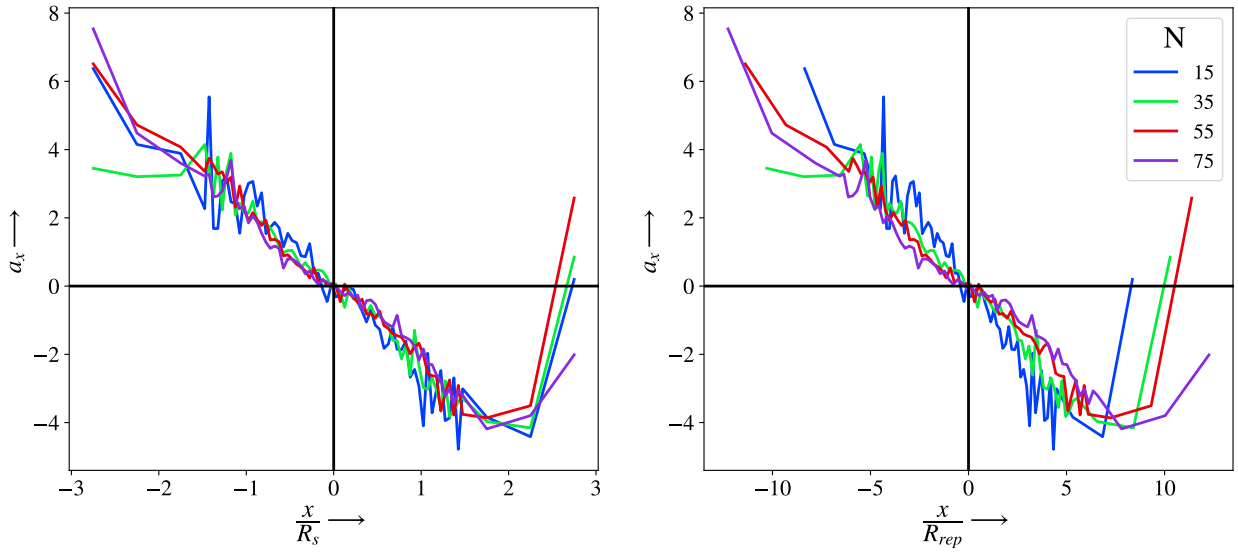

Figure 3.6: Mean value of x-component of acceleration as a function of x away from the swarm's center. Here, different colors represent swarms of different numbers. Note that each swarm shows the linear relation of acceleration about the center of the swarm. For a comparison with natural swarms, see Figure B.1.

3.2.2 SPRING CONSTANT

Following the previous section, we can extract and compare the scaling of the spring constant with the size of the swarm. Figure 3.6 shows acceleration vs position curve for swarms with different particle numbers. The left plot shows that if we normalize position by the radius of the swarm, the curves seem to superimpose, although they don't, but contrasting it with the right plot shows that there is a dependence of the spring constant on the radius of the swarm. Explicitly, for the same set of runs that produced Figure 3.6, the relation is given in Figure 3.7. The spring constant is calculated within the $0.5R_S$ region.

The result is qualitatively similar to the behavior observed in natural swarms(Figure B.2). The spring constant is inversely proportional to the radius of the swarm. However, the exponent is different from both the natural swarms and the adaptive gravity swarms. We will discuss this exponent when we discuss the effect of parameters on various relations in section 3.3.

Even though the exponent varies, the inverse relation of κ and R_S is present in all different simulations. This marks the importance of adaptivity in forming the swarms. In a system with pure gravity, where force follows inverse square law, i.e., $F_{ij} = Cr_{ij}^{-2}$ and no attenuation factor, with uniform density, we can get a harmonic relation such that $F_{\text{eff}} \propto -r_i$. However, the spring constant extracted from such a relation would not depend on the size of the swarm. To get to a behavior where the spring constant decreases as size increases, adaptivity is thus crucial. Adaptivity implies that as numbers in the center increase, the proportion of the force experienced becomes smaller, thereby making the force smaller, and for the same distance, the spring constant weaker.

3.2.3 ACCELERATION AND VELOCITY STATISTICS

Figure 3.8 shows the probability distribution of the x-component of acceleration of the particles in the swarm. The results are different for natural and adaptive gravity swarms– their distributions are close to Gaussian for very small accelerations but show heavy, exponential tails for large accelerations. However, all three swarm types have acceleration distributions independent of the swarm size.

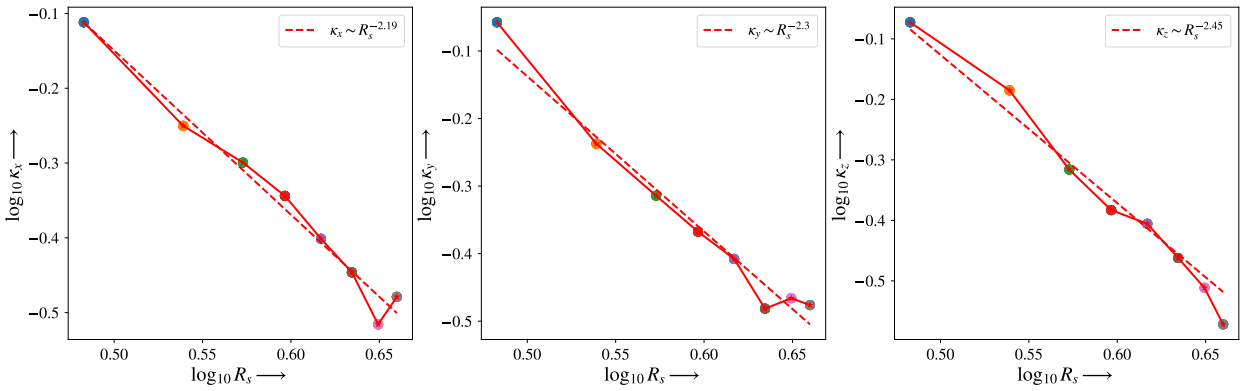

Figure 3.7: Spring constant calculated using acceleration spatial distribution as a function of swarm size. Using linear regression (dashed line), we calculate the exponent of scaling given in the top right box. For a comparison with natural swarms, see Figure B.2.

Similarly, Figure 3.11c shows the probability distribution of the x-component of the velocity of the particles in the swarm. Here, the trend is similar to natural and adaptive gravity swarms- as the swarm size increases, the velocity distributions also develop a long tail. However, for natural swarms, larger swarms had heavier tails. See Figure 3.11d.

Figure 3.9a shows the spatial distribution of the velocities of the particles in the swarm. It depicts the average speed of midges as a function of the distance away from the center of mass of the swarm. The figure shows that the average speed at a position is constant. This also implies that the mean kinetic energy of a midge is constant in space and time(Figure 3.2). The uniformity of the velocity profile across the swarm serves is similar to natural swarms. In [17], only adaptive gravity could reproduce, whereas Newtonian gravity could not, showing that adaptivity along with long-range interaction potential is required to produce this(Figure B.3).
We observe this similar trend in natural swarms as well as in the adaptive gravity model for self-propelled particle swarms for the standard deviation of the speed of midges as a function of the distance away from the center of mass of the swarm (Figure 3.9b).

Figure 3.10 shows the mean value of the x-component of the acceleration versus the speed normalized by mean speed. The red values of the plot represent the mean value of the x-component of the acceleration versus the speed normalized by the mean speed taken in region $x > 0$ or the right hemisphere. The blue values of the plot represent the mean value of the x-component of the

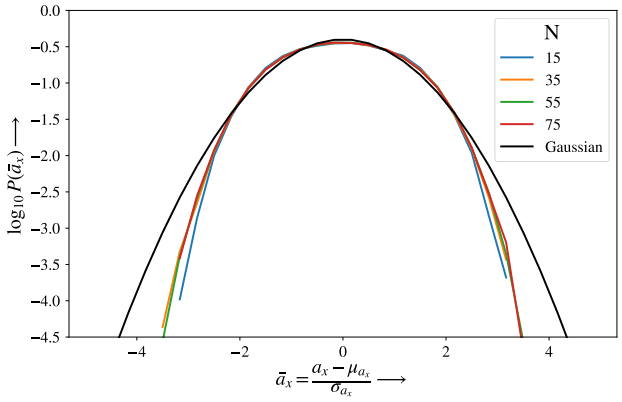

Figure 3.8: The distribution of the x-component of the acceleration normalized by its mean and standard deviation for different simulated swarms. A reference Gaussian curve is shown in black. For a comparison with natural swarms, see Figure B.1.

acceleration versus the speed normalized by the mean speed taken in the region $x < 0$ or the blue hemisphere. Taken for the swarm as a whole, i.e., summing right and left hemispheres would give us the black values. This result is very similar for natural swarms; however, the magnitude of acceleration in each hemisphere is slowly increasing with velocity(Figure B.5).

3.2.4 SCALING

In this section, we look at three significant scaling– number, density at the swarm center, and velocity kurtosis are compared with swarm radius. All three are increasing functions of swarm radius. Although the adaptive gravity model produced this positive dependence, the adaptive gravity model for self-propelled particles shows a much stronger scaling. (Figure B.6 and Figure 3.11)

Figure 3.11a shows that the number of particles increases on increasing the swarm radius. Although we get the latter from the former, as we use the number of particles as a simulation parameter, the data is presented in such a way because we can relate it to gravitational systems– the number is equivalent to mass. Therefore, according to the figure, a bigger swarm size implies a higher mass. This is counterintuitive as, on increasing mass, a pure gravity system with a higher mass *ceteris paribus* would decrease in size due to a higher mutual interaction, but this is not so for adaptive gravity systems as adaptivity would pacify the additional mutual force. It is crucial to point out that for adaptive gravity swarms, the increase in number with swarm radius is caused by

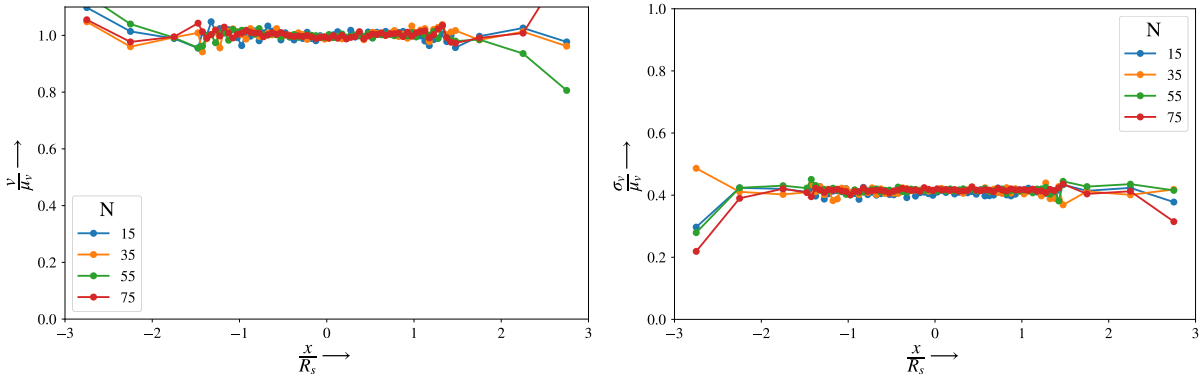

(a) (b)

Figure 3.9: Figure 3.9a shows mean speed v normalized by the speed at the center v_c, as a function distance from the center of the swarm normalized by R_S. Speed v is uniform with position. Figure 3.9b shows the standard deviation of the speed σ_v normalized by the average speed in the swarm μ_v as a function of the distance from the center of mass normalized by R_S. Note the same uniformity for the standard deviation of the speed with position. For a comparison with natural swarms Figure B.3 and Figure B.4.

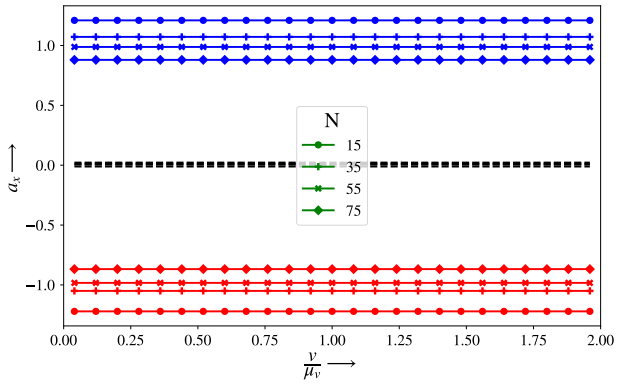

Figure 3.10: The mean value of the x-component of the acceleration versus the speed v, normalized by the average speed μ_v, of the left hemisphere ($x < 0$) (blue), right hemisphere ($x > 0$) (red), and both hemispheres (black). The overall acceleration (black lines) is close to zero. Symbols in green represent the number of particles for blue and red lines. For our simulations, acceleration is independent of speed. On increasing particle numbers, the magnitude of acceleration decreases. For a comparison with natural swarms, see Figure B.5.

short-range repulsion and cannot be produced by long-range adaptive gravity only.

Although the adaptive gravity model for self-propelled particles produces stronger scaling, it is still not in the regime of natural swarms. For natural swarms, $\frac{\Delta \log N}{\Delta \log R_S} \approx 1.3$ whereas for the simulated swarm in Figure 3.11a $\frac{\Delta \log N}{\Delta \log R_S} \approx 3.7$. So, in these simulated swarms, the radius increases slowly with number than for natural swarms.

In Figure 3.11b $\tilde{\rho}$ is the density, whereas $\tilde{\rho}_0$ is the density at the center. It was extracted by fitting a Gaussian to $0.5R_S$ region of the density profile (Figure 3.12a). However, we find a worse agreement between the adaptive gravity model for self-propelled particle swarms and natural swarms. It resembles the result of adaptive gravity swarms. For natural swarms, $\frac{\Delta \log \tilde{\rho}_0}{\Delta \log R_S} \approx -1.7$, whereas for simulation, it is $\frac{\Delta \log \tilde{\rho}_0}{\Delta \log R_S} \approx +0.6$. For natural swarms, density at the center falls with swarm size; however, our simulated swarms increase weakly with swarm size.

In Figure 3.11d α_4 represents kurtosis of the x-component of velocity, which is the fourth moment. It is concerned with the extent to which a distribution's tails differ from the tails of a normal distribution. A higher kurtosis means a higher, sharper peak and thicker, fatter tails, indicating more data in the tails than a normal distribution. The formula for kurtosis used here is:

$$\alpha_4 = \frac{N(N+1)}{(N-1)(N-2)(N-3)} \sum_{i=1}^{N} \left(\frac{v_{x,i} - \mu_{v_x}}{\sigma_{v_x}} \right)^4 - \frac{3(N-1)^2}{(N-2)(N-3)} \tag{3.5}$$

Here, $v_{x,i}$ represents the x-component of velocity of i^{th} individual, μ_{v_x} is the expectation value of $v_{x,i}$, σ_{v_x} is the standard deviation of $v_{x,i}$. This formula is used when the dataset size is small. For a normal distribution with zero mean and unit variance, α_4 would be 0.

The natural swarms have a high kurtosis greater than zero, i.e., heavier tails than a Gaussian. Their kurtosis also increases with swarm radius, albeit the increase is slow, and kurtosis remains almost constant for larger swarms, about 150 to 200 mm(Figure B.1). The figure captures this asymptotic behavior perfectly- as the swarm size increases, the velocity distributions also develop a long exponential tail, more conspicuously than adaptive gravity swarms. However, the kurtosis is less than zero, implying that the tails are lighter than those of a Gaussian. See Figure 3.11c.

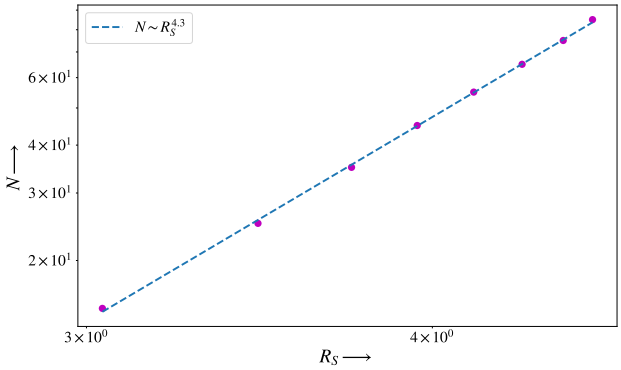

(a)

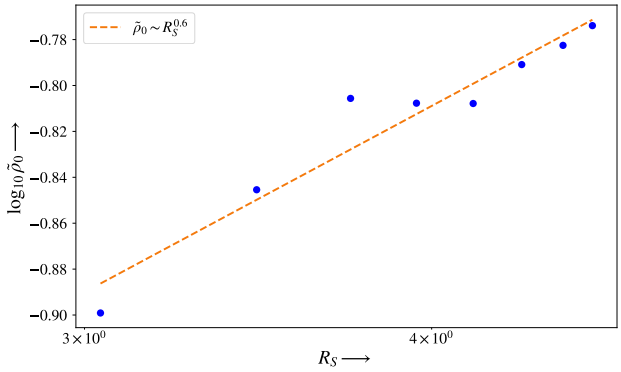

(b)

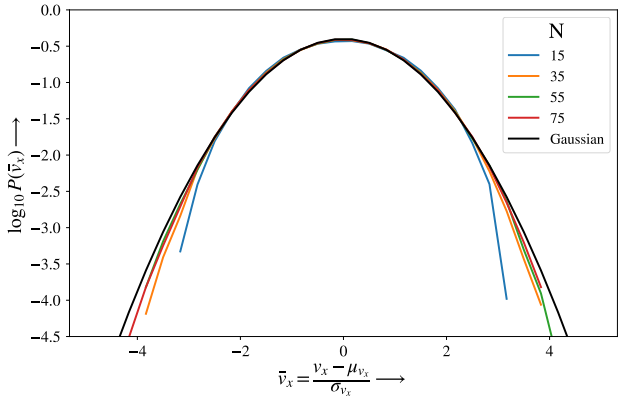

(c)

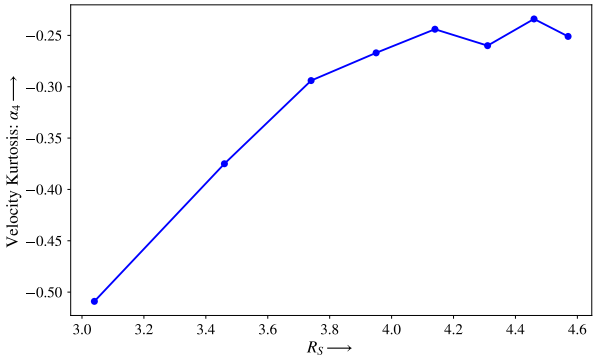

(d)

Figure 3.11: 3.11a shows the scaling of particle number with swarm size with the exponent of scaling in the top right corner. 3.11b shows the scaling of number density with swarm size with exponent in the top right box. 3.11d shows velocity kurtosis as a function of swarm size. Zero kurtosis implies a Gaussian distribution. 3.11c distribution of the x-component of the velocity normalized by its mean and standard deviation for different simulated swarms. A reference Gaussian curve is shown in black. For a comparison with natural swarms, see Figure B.6.

3.2.5 DENSITY

In natural swarms, the density profile near the swarm's center resembles a Gaussian. This is also true for our simulations (Figure 3.12a). The density profile on normalizing the distance by R_S shows similar curves and a clear dependence on R_S.

Figure 3.12b is a contour plot of probability density where white is the region with the highest probability density while black has zero probability density, and the gradient of color represents the gradient of probability density. The figure shows a Gaussian density profile in action– the central region of the highest density that falls quickly as we move away from the center.

3.3 EFFECT OF PARAMETERS

In previous sections, we show that the adaptive gravity model for self-propelled particles can reproduce various relations characterizing natural swarms. These were robustly shown for the adaptive gravity model, so we bring over the same relations. In the following section, we observe the effect of parameters on these relations for swarming particles.

The main dynamics equation can be rewritten as:

$$\frac{1}{v_0\beta}\frac{d\vec{v}}{dt} \equiv \frac{d\vec{v}}{d\tau} = -\left(\frac{\vec{v}}{v_0} - \hat{n}\right) + \frac{1}{v_0\beta}\vec{\varepsilon} \tag{3.6}$$

So the interesting quantity to compare is- noise multiplied by relaxation time divided by self-propulsion speed ($\frac{\varepsilon}{v_0\beta}$). We vary v_0; however, in principle, we could vary either of the three parameters- ε, v_0, β and change the ratio and observe similar dynamics.

Additionally, we can also vary parameters in $\hat{n}$ which would be- size of particle (R_{rep}) and range of adaptivity (R_{ad}). We ignore the size of the simulation arena (R_{marker}) as it becomes only relevant when particle/swarm reaches the edges of the simulation box, which not only seldom happens and when it happens, it doesn't affect swarm's emergent dynamics as it affects the all the individuals in a similar manner and so would be subtracted out in internal dynamics.

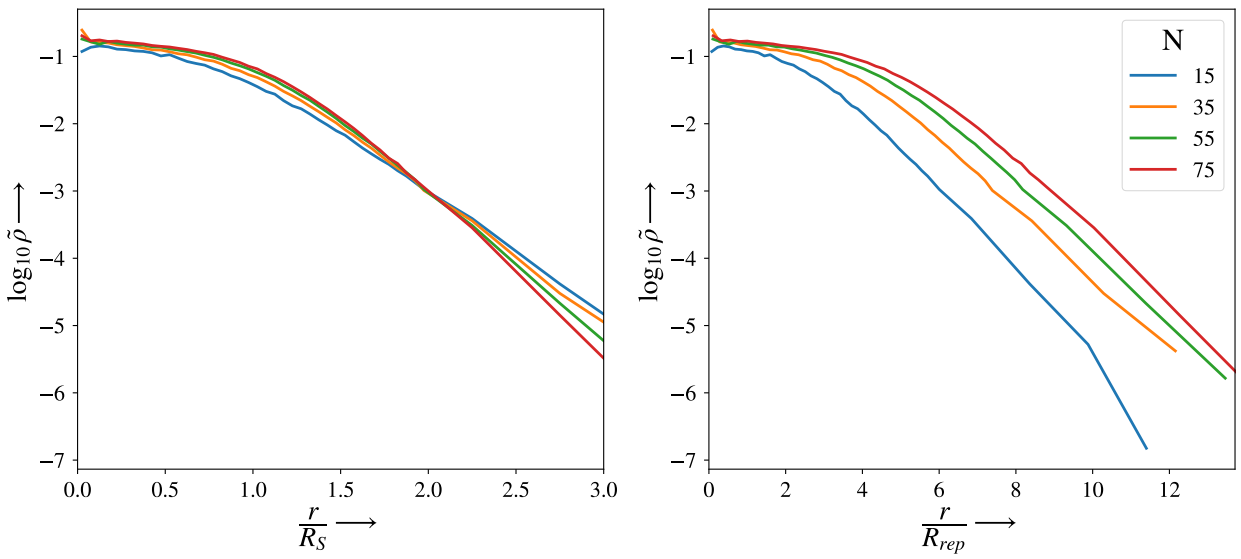

(a)

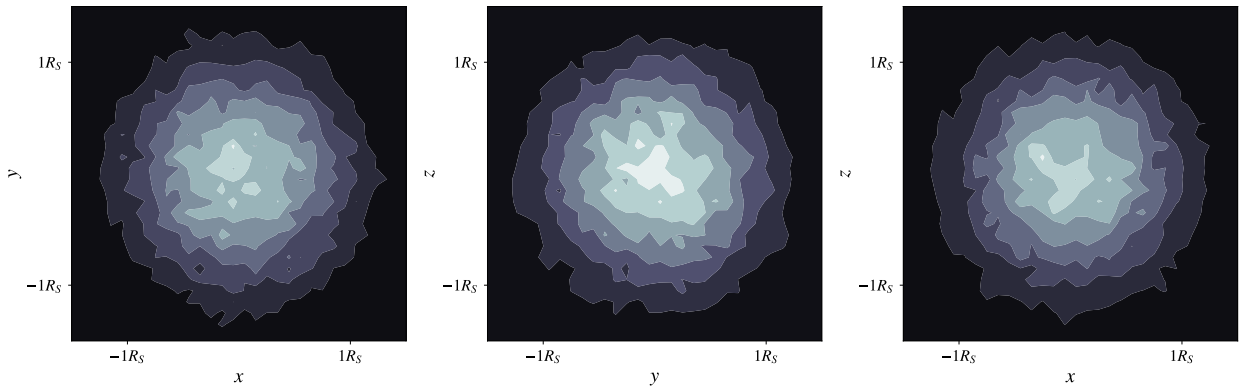

(b)

Figure 3.12: 3.12a shows number density profile $\tilde{\rho}$ as a function of distance from the center normalized by swarm size (left) and particle size (right). 3.12b is a contour plot showing the density profile in 3D– light to dark is a decreasing density gradient. For a comparison with natural swarms, see Figure B.7.

3.3.1 PARTICLE SIZE

This section presents the result of increasing particle size, keeping all other parameter values constant. To contrast the effect of increasing and decreasing R_{rep}, we present results from two different simulations with $R_{\text{rep}} = 0.5$ and 1.5, respectively. See Figure 3.13 and 3.14.

We start by comparing the scaling of particle number with swarm radius. (Figure 3.13a and 3.14a)

$$\left.\frac{\Delta \log N}{\Delta \log R_S}\right|_{R_{\text{rep}}=0.5} \approx 7.0$$

$$\left.\frac{\Delta \log N}{\Delta \log R_S}\right|_{R_{\text{rep}}=1.5} \approx 3.7$$

On increasing particle size, particle number scales weakly with swarm size.

Figure 3.13e and 3.14e show density profile. As we increase particle size, we get a larger region of constant density about the center of the swarm. Additionally, increasing particle size also decreases density magnitude. We also compare the scaling of density at the center with the swarm radius. (Figure 3.13f and 3.14f)

$$\left.\frac{\Delta \log \tilde{\rho}_0}{\Delta \log R_S}\right|_{R_{\text{rep}}=0.5} \approx +2.8$$

$$\left.\frac{\Delta \log \tilde{\rho}_0}{\Delta \log R_S}\right|_{R_{\text{rep}}=1.5} \approx +0.3$$

On increasing particle size, density at the center scales weakly with swarm size.

Figure 3.13b and 3.14b show distance with the closest neighbor as a function of distance from the center normalized by particle size and swarm size, respectively. For $R_{\text{rep}} = 0.5$ the minima occurs around $2R_{\text{rep}}$ while for $R_{\text{rep}} = 1.5$ the minima occurs around $1.5R_{\text{rep}}$. Therefore, particles come closer (relatively) with increasing particle size.

Figure 3.13c and 3.14c are acceleration vs position plots for the x-component. Changing particle size doesn't affect the magnitude of acceleration; however, it does change the shape of the acceleration profile. For $R_{\text{rep}} = 0.5$, the function appears curving downwards away from the center, whereas for $R_{\text{rep}} = 1.5$, it appears to curve slightly upwards. This also affects the spring constant calculations. Figure 3.13d and 3.14d show spring constants and their scaling in upper-right. Even

though the particle size doesn't affect the magnitude of the spring constant, it does affect the scaling. The curves in the red represent spring constant calculated by fitting acceleration within $0.5R_S$ region, while the blue are calculated by fitting acceleration within $1.0R_S$ region. For $R_{\text{rep}} = 0.5$, the blue spring constant is lower than the red spring constant, which shows that the slope nearer to the center is higher than the slope away from it– an indirect verification for concave acceleration profile. This trend is exactly the opposite for $R_{\text{rep}} = 1.5$ as its acceleration profile is convex. For comparing scaling, we would stick to the red spring constant.

$$\left.\frac{\Delta \log \kappa_x}{\Delta \log R_S}\right|_{R_{\text{rep}}=0.5} \approx -2.5$$

$$\left.\frac{\Delta \log \kappa_x}{\Delta \log R_S}\right|_{R_{\text{rep}}=1.5} \approx -1.5$$

On increasing particle size, the spring constant scales weakly with swarm size.

Figure 3.13g and 3.14g represent kurtosis of v_x. In this aspect, there is not much difference in increasing particle size.

An additional aspect to compare is the size of the swarm relative to the size of the particle. For $R_{\text{rep}} = 0.5$ let $R_S = 2.6$ be the typical size of the swarm then

$$\left.\frac{R_S}{R_{\text{rep}}}\right|_{R_{\text{rep}}=0.5} = 4.2$$

Similarly for $R_{\text{rep}} = 1.5$ let $R_S = 5.0$ be the typical swarm size then

$$\left.\frac{R_S}{R_{\text{rep}}}\right|_{R_{\text{rep}}=1.5} = 3.4$$

On increasing particle size, we get smaller swarms relative to particle size, even though the absolute size of the swarm increases.

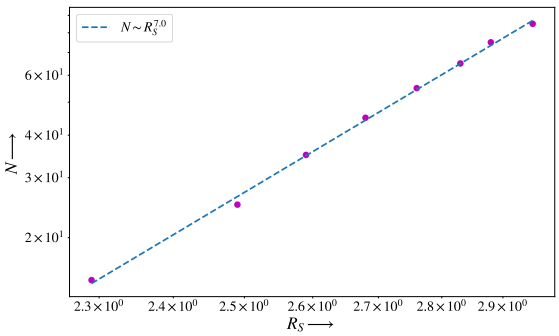

(a) Number vs swarm size

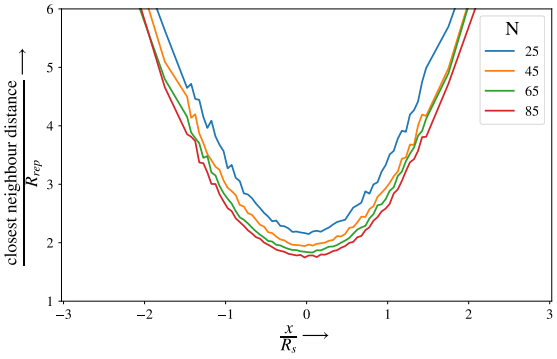

(b) Closest neighbor distance vs position

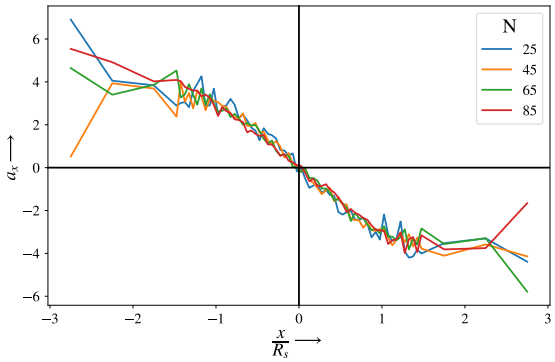

(c) Acceleration vs position

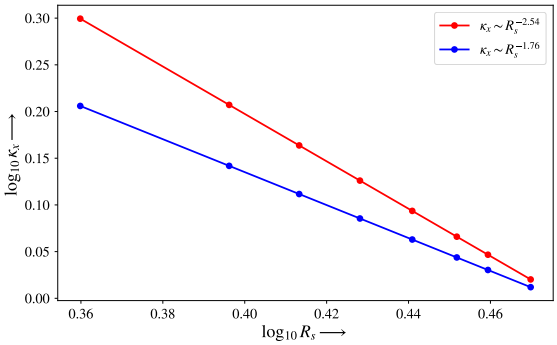

(d) Spring constant vs swarm size

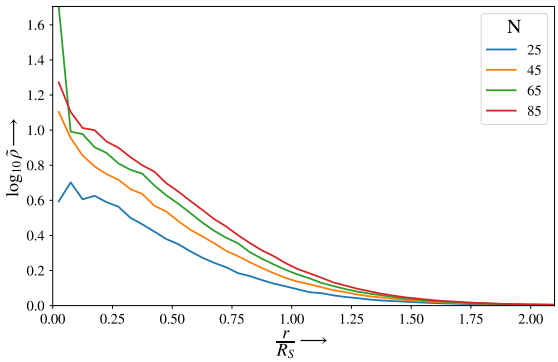

(e) Density profile

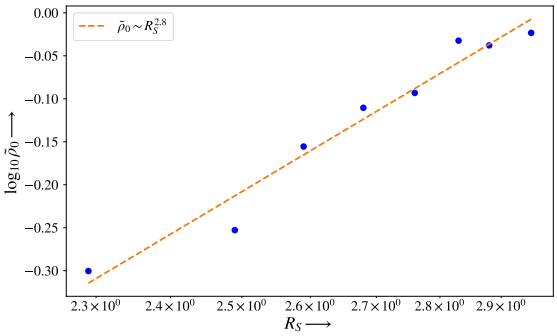

(f) Density at center vs swarm size

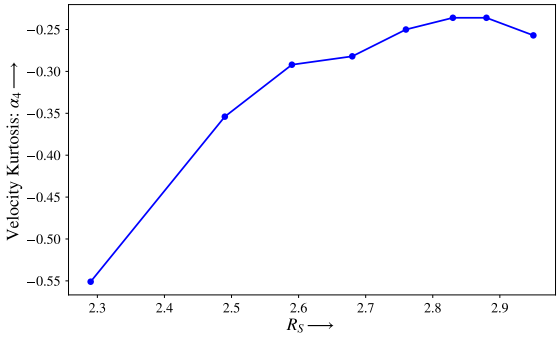

(g) Kurtosis vs swarm size

Figure 3.13: $R_{\text{rep}} = 0.5$

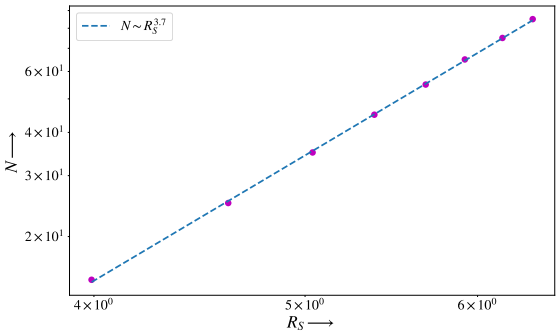

(a) Number vs swarm size

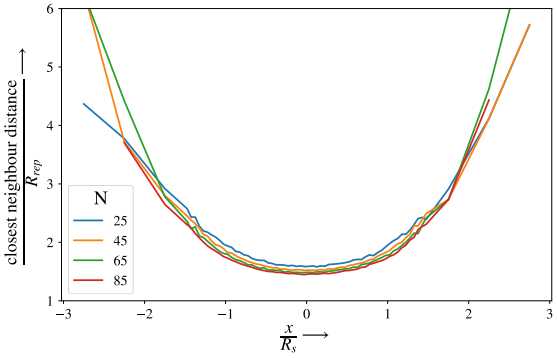

(b) Closest neighbor distance vs position

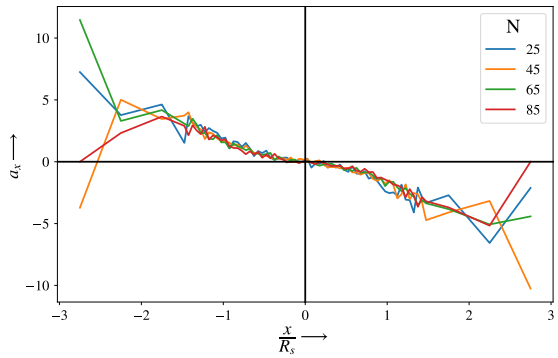

(c) Acceleration vs position

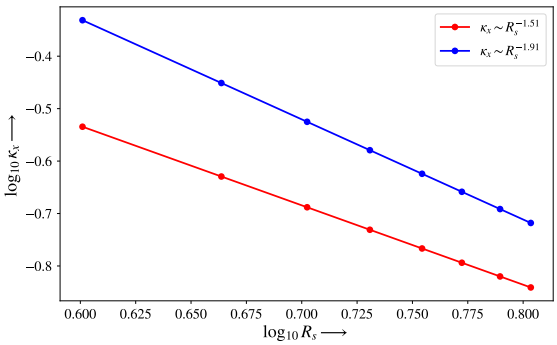

(d) Spring constant vs swarm size

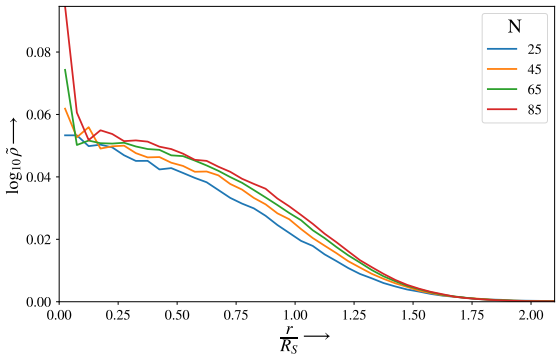

(e) Density profile

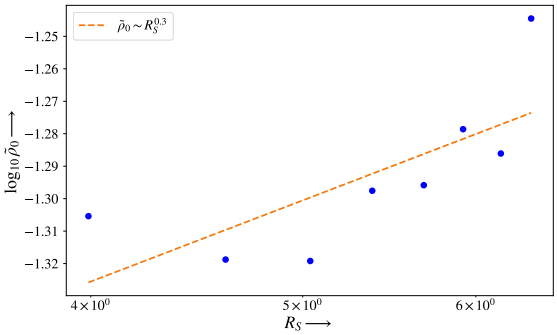

(f) Density at center vs swarm size

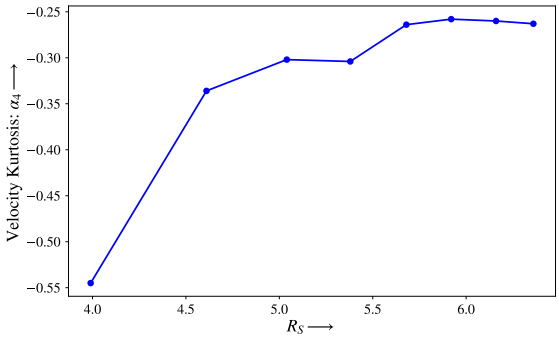

(g) Kurtosis vs swarm size

Figure 3.14: $R_{\text{rep}} = 1.5$

3.3.2 SELF-PROPULSION SPEED

In this section, we present the result of increasing self-propulsion speed, keeping all other parameter values constant. To contrast the effect of increasing and decreasing v_0, we present results from two simulations with $v_0 = 2.5$ and 7.5, respectively. See Figure 3.15 and 3.16.

We start by comparing the scaling of particle number with swarm radius. (Figure 3.15a and 3.16a)

$$\left.\frac{\Delta \log N}{\Delta \log R_S}\right|_{v_0=2.5} \approx 7.1$$

$$\left.\frac{\Delta \log N}{\Delta \log R_S}\right|_{v_0=7.5} \approx 3.8$$

On increasing speed, particle numbers scale weakly with swarm size.

Figure 3.15e and 3.16e show density profile. As we increase speed, we get a larger region of constant density about the swarm's center. Additionally, increasing speed also increases density magnitude, albeit this increase is small. We also compare the scaling of density at the center with the swarm radius. (Figure 3.15f and 3.16f)

$$\left.\frac{\Delta \log \tilde{\rho}_0}{\Delta \log R_S}\right|_{v_0=2.5} \approx +3.0$$

$$\left.\frac{\Delta \log \tilde{\rho}_0}{\Delta \log R_S}\right|_{v_0=7.5} \approx +0.3$$

On increasing speed, density at the center scales weakly with swarm size.

Figure 3.15b and 3.16b show distance with the closest neighbor as a function of distance from the center normalized by particle size and swarm size, respectively. For $v_0 = 2.5$ the minima occurs around $2R_{\text{rep}}$ while for $v_0 = 7.5$ the minima occurs around $1.5R_{\text{rep}}$. Therefore, particles come closer (relatively) with increasing particle size.

Figure 3.15c and 3.16c are acceleration vs position plots for the x-component. In contrast to the effect of particles, changing speed affects the magnitude of acceleration as well as the shape of the acceleration profile. Increasing self-propulsion speed increases acceleration within $1R_S$- for $v_0 = 2.5$, it is typically about 1, whereas for $v_0 = 7.5$, acceleration is typically around 5. For

$v_0 = 2.5$, the function appears to curve downwards away from the center, whereas for $v_0 = 7.5$, it appears to curve upwards. This also affects the spring constant calculations. Figure 3.15d and 3.16d show spring constants. The spring constant for $v_0 = 2.5$ is constant about $10^{-0.6}$, whereas for $v_0 = 7.5$, it is higher and spread over a larger range. The color scheme and scaling are as present in subsection 3.3.1. For $v_0 = 2.5$, the blue spring constant is equal to the red spring constant as the acceleration profile is near constant even within $1R_S$ region and curves only later. This trend differs for $v_0 = 7.5$ as its acceleration profile convex- red spring constant is lower than the blue spring constant. For comparing scaling, we would stick to the red spring constant. I will omit the scaling for $v_0 = 2.5$ as the swarm radius range is smaller, and the red spring constant and blue constant are very close in values but with very different scaling.

$$\left.\frac{\Delta \log \kappa_x}{\Delta \log R_S}\right|_{v_0=7.5} \approx -2.2$$

We cannot conclude about the effect of speed on scaling.

Figure 3.15g and 3.16g represent kurtosis of v_x. Here, just like particle size, speed doesn't show much effect on kurtosis.

An additional aspect to compare is the size of the swarm relative to the size of the particle. For $v_0 = 2.5$ let $R_S = 5.7$ be the typical size of the swarm then

$$\left.\frac{R_S}{R_{\text{rep}}}\right|_{v_0=2.5} = 5.7$$

Similarly for $v_0 = 7.5$ let $R_S = 3.1$ be the typical swarm size then

$$\left.\frac{R_S}{R_{\text{rep}}}\right|_{v_0=7.5} = 3.1$$

On increasing self-propulsion speed, we get smaller swarms relative to particle size, along with a decrease in the absolute size of the swarm.

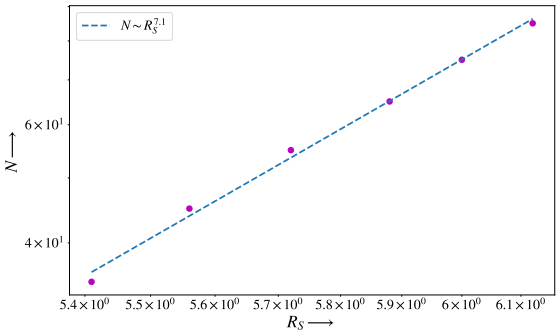

(a) Number vs swarm size

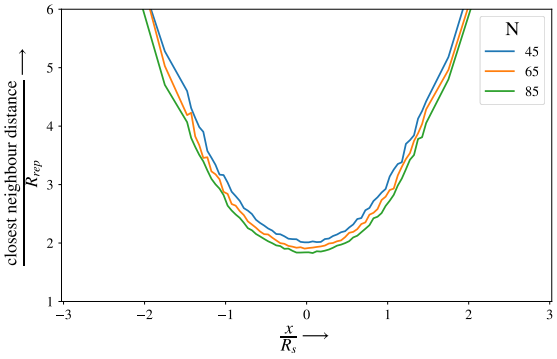

(b) Closest neighbor distance vs position

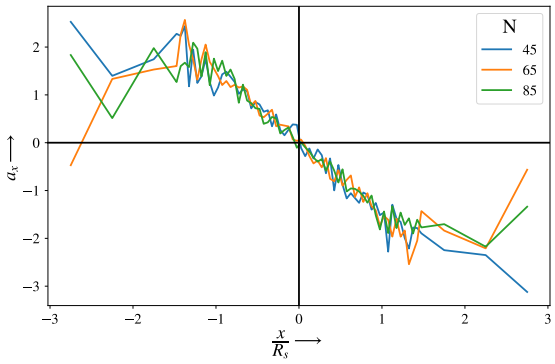

(c) Acceleration vs position

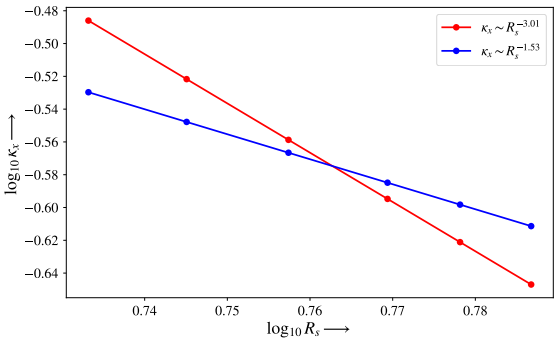

(d) Spring constant vs swarm size

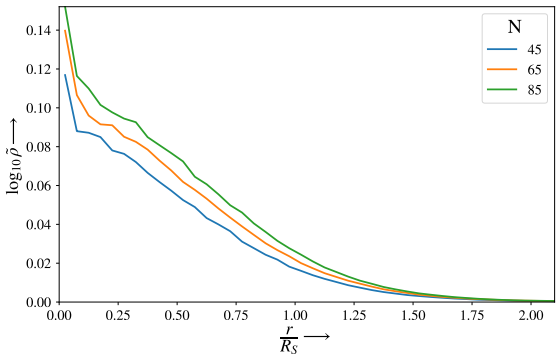

(e) Density profile

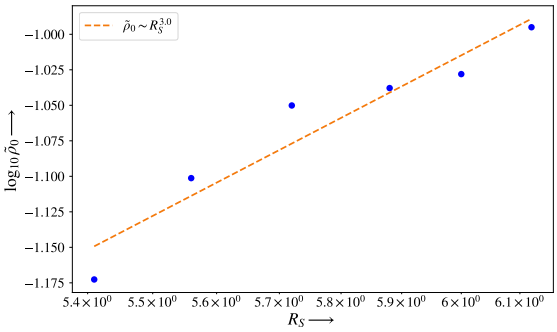

(f) Density at the center vs swarm size

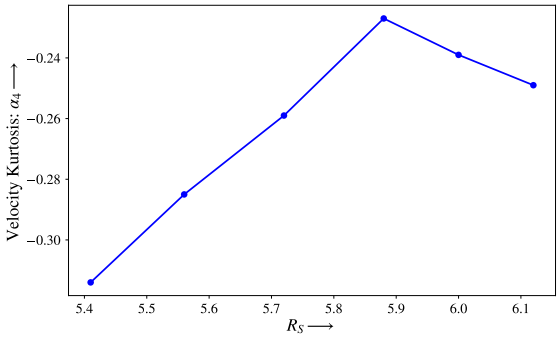

(g) Kurtosis vs swarm size

Figure 3.15: $v_0 = 2.5$

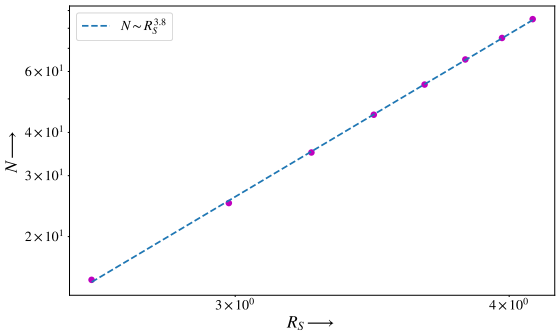

(a) Number vs swarm size

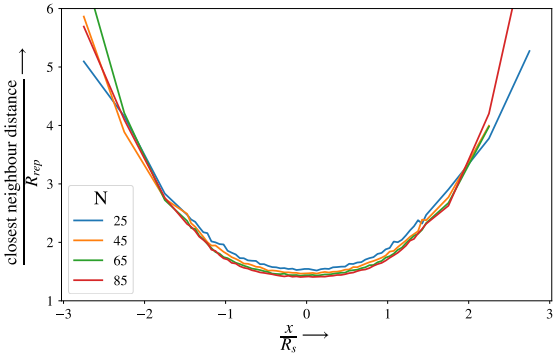

(b) Closest neighbor distance vs position

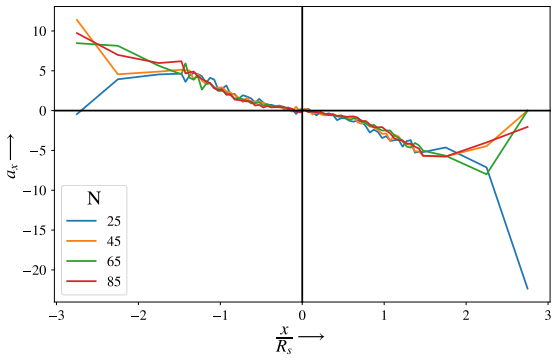

(c) Acceleration vs position

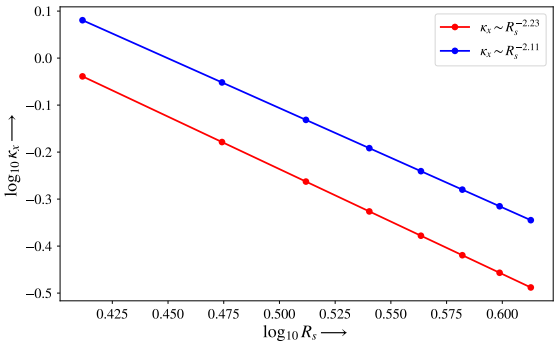

(d) Spring constant vs swarm size

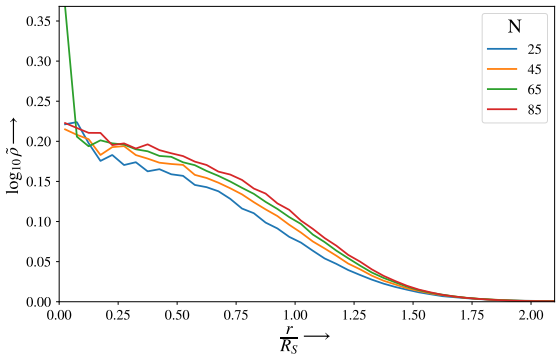

(e) Density profile

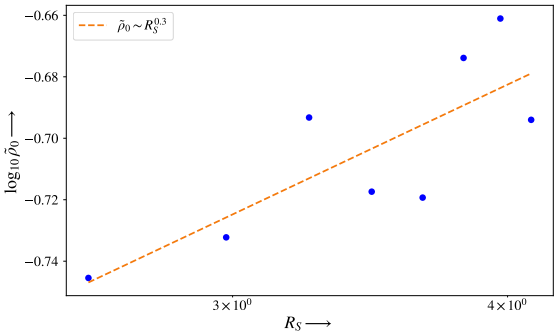

(f) Density at center vs swarm size

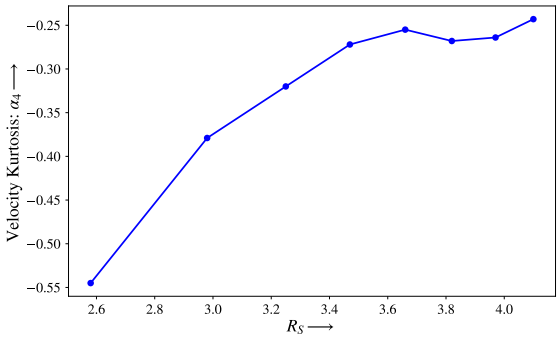

(g) Kurtosis vs swarm size

Figure 3.16: $v_0 = 7.5$

3.3.3 NOISE

We presented results on changing two parameters- particle size and self-propulsion speed. In this section, we present an interpretation of these results. The trends observed when increasing particle size are very similar to those observed when increasing speed. The only trend that doesn't match is the number vs swarm radius plot. On increasing particle size, you get bigger swarms; on increasing speed, you get smaller swarms. However, this is not counterintuitive if we choose to compare swarm sizes directly rather than swarm size relative to particle size. When this quantity is compared, both show a similar trend- increasing particle size/speed decreases relative swarm size. The major changes in increasing particle size/speed are:

- Decreasing R_S/R_{rep}
- Weaker scaling of number with swarm size or stronger scaling of swarm size with the particle number
- Relative closer nearest neighbor distance
- Weaker (albeit positive) scaling of number density at the center with swarm size.
- Independence of kurtosis trend.

The effect of increasing particle size/speed is equivalent to decreasing noise (equation 3.6). Decreasing noise brings the swarm relatively closer as there are smaller fluctuations about the swarm center. Smaller noise implies there is a tighter swarm with smaller fluctuations since there is not much leeway to add additional particles, so swarm size increases much faster when adding additional particles. Additionally, particles are also relatively closer to decreasing noise– indirect evidence for the previous statement. This tightness within the center also implies that the number density is primarily saturated and increases very slowly with increasing particle numbers (equivalent to increasing swarm size).

We also observe that we reach regimes similar to those observed in the natural swarms on changing parameters. This shows that the model can successfully replicate natural swarms and produce a coherent swarm with an oscillator-like behavior for a more extensive range of parameter values

than observed in the natural systems. We hypothesize that natural systems are restricted to such a small section of the parameter space because these sets of parameters produce the most optimized swarms. However, it is hard to infer what these swarms are optimizing. Our simplest guess is that the insects or swarms are optimizing for exploration while trying to maintain a uniform probability density around the center. Increasing noise increases exploration; however, it decreases the region of uniform probability around the center, so the swarms globally settle midway between these two. There are some ambiguous trends in the above comparison:

- Decreasing number density. However, this trend is the opposite of self-propulsion speed.
- Weaker scaling of spring constant with swarm size. However, this is not observed for self-propulsion speed.

3.4 PAIR FORMATION

In addition to steady-state features, recent observations have found evidence for the dynamic formation of synchronized pairs of midges, which typically oscillate with respect to each other at a higher-than-normal frequency and maintain a small distance between them. At the same time, they move together through the swarm. Pairs were identified in the laboratory swarms by analyzing the relative distance between pairs of midges as they moved through the swarm. The relative distance between any two unpaired midges exhibits oscillations with an amplitude on the order of the swarm radius and a period on the order of the typical time it takes a midge to fly across the swarm. Such behavior is typical of unpaired midges. However, the relative distance between the midges occasionally exhibited small-amplitude high-frequency oscillations (compared with the unpaired state). When these oscillations had a frequency that was higher than a threshold value and persisted longer than a threshold time (with both thresholds estimated using measured characteristics of the swarms), the two midges were identified as a pair. Note that during pairing, the amplitude of the relative oscillations of the pair diminished but remained much larger than the distance where midges might accelerate away from each other to avoid collision. It is not known if the pairing results from additional, more complex behavioral rules or whether it can arise naturally as a passive by-product of swarming. The adaptive gravity model was able to reproduce this behavior success-

fully without any modifications. Thus, pairing can be viewed as an emergent phenomenon and a natural outcome of the same interactions that lead to swarm formation.

To identify unique patterns of behavior in these paths for natural swarms, a time-frequency analysis utilizing the continuous wavelet transform (CWT) with Morlet wavelets[20]. The signal for this CWT was taken to be the distance between two midges r_{ij}. Then they considered all midge pairs and isolated segments of the trajectories where the CWT of $r_{ij}(t)$ had significant power P at high frequencies (above $\sim 1Hz$) and not at low frequencies (below $\sim 1Hz$), where the threshold of $1Hz$ comes from dividing swarm diameter by mean speed. The pairs were defined differently for adaptive gravity simulations since we could take advantage of the additional information we have in the simulations to relate the pairing to the energetics of the particle pair, which is physically more meaningful. Their results matched with the natural swarms too[18](Figure B.8). We reproduced their metrics below.

Let $V_{\text{pair}}(r_{ij})$ be the effective two-body potential bet particles i, j with distance r_{ij}.

$$V_{\text{pair}}(r_{ij}) = \frac{1}{\gamma\sqrt{R_{\text{ad}}^2 + \alpha^2\gamma^2}}\left[\arctan\left(\frac{\gamma r_{ij}}{\sqrt{R_{\text{ad}}^2 + \alpha^2\gamma^2}}\right) - \frac{\pi}{2}\right] \tag{3.7}$$

Here $\gamma = 0.5[\gamma(r_i) + \gamma(r_j)]$, where $\gamma(r_i)$ is:

$$\gamma(r_i) = \sqrt{1 + R_{\text{ad}}^2 I_{\text{bg}}(r_i)}$$

Here, I_{bg} is the background sound intensity.

$$I_{\text{bg}}(r_i) = \sum_{k\neq i,j}^{n} \frac{1}{r_{ik}^2 + \alpha^2} \tag{3.8}$$

Additionally, the kinetic energy T_{pair} for the pair i, j is:

$$T_{\text{pair}}(r_{ij}) = \frac{1}{4}\dot{r}_{ij}^2 \tag{3.9}$$

The criteria for defining bounded pair is as follows:

$$T_{\text{pair}} + V_{\text{pair}} \leq 0 \implies \frac{T_{\text{pair}}}{|V_{\text{pair}}|} \leq 1 \tag{3.10}$$

If for the time duration $\tau_{\text{bd}} = 4R_S/v_0$ for a pair i, j, the absolute ratio for kinetic energy to potential energy is less than, i.e., $|T_{\text{pair}}/V_{\text{pair}}| < 1$, then that pair is said to be bounded.

The adaptive gravity model for self-propelled particles also shows pairs, which, in summary, are high-frequency, low-amplitude oscillations in r_{ij} for a characteristic time duration. See Figure 3.17. However, the criterion defined for the bounded pair above doesn't work for the adaptive gravity model for self-propelled particle simulations. The bounded pair trajectory shown below does show a very small value for energy ratio, but it is not less than unity. See Figure 3.18.

We try to develop analytical criteria, following the similar method as shown above, even though we cannot calculate the potential like it was done in equation 3.7. But we can try to numerically develop a criterion. We start with our equation 2.5:

$$\frac{d\vec{v}_i}{dt} = -\beta(\vec{v}_i - v_0\hat{n}_i)$$

We multiply with $\vec{v}_i$:

$$\vec{v}_i \cdot \frac{d\vec{v}_i}{dt} = -\beta(\vec{v}_i \cdot \vec{v}_i - v_0\vec{v}_i \cdot \hat{n}_i) \implies \frac{d\frac{1}{2}v_i^2}{dt} = -\beta(v_i^2 - v_0\vec{v}_i \cdot \hat{n}_i) \tag{3.11}$$

We rewrite $\frac{1}{2}v_i^2 = T_i$ as kinetic energy for particle i.

$$\frac{dT_i}{dt} = -\beta(2T_i - v_0\vec{v}_i \cdot \hat{n}_i) \tag{3.12}$$

Here, $\vec{n}_i = \vec{F}_i$. Here, this $\vec{F}_i$ is the same as adaptive gravity force $\vec{F}_{\text{adaptive},i}$ in equation 2.8. We can rewrite this as:

$$\frac{dT_i}{dt} - \beta v_0\vec{v}_i \cdot \hat{F}_i = -2\beta T_i \implies \frac{dT_i}{dt} + \frac{dV_i}{dt} = -2\beta T_i \implies \frac{dE_i}{dt} < 0 \tag{3.13}$$

We take $dV_i = -\beta v_0 \hat{F}_i \cdot \vec{dr}_i$, as an effective potential; and $E_i = T_i + V_i$. Because of the dissipative component $-\beta\vec{v}$ in the acceleration, we don't have conservation of energy, and the total energy decreases with time.

For a bounded pair i, j force acts in the direction from particle i to j. Therefore, $\hat{n}_i = \hat{F}_i = \hat{r}_{ij}$. So we get:

$$\frac{dT_i}{dt} = -\beta \left(2T_i - v_0 \vec{v}_i \cdot \hat{r}_{ij}\right) \tag{3.14}$$

Adding this with a similar equation for particle j gives:

$$\frac{d(T_i + T_j)}{dt} = -\beta \left(2(T_i + T_j) - v_0(\vec{v}_i \cdot \hat{r}_{ij} + \vec{v}_j \cdot \hat{r}_{ji})\right) \tag{3.15}$$

This can be equivalently written as:

$$\frac{dT_{ij}}{dt} = -\beta \left(2T_{ij} - v_0(\vec{v}_i - \vec{v}_j) \cdot \hat{r}_{ij}\right) = -\beta \left(2T_{ij} - v_0 \vec{v}_{ji} \cdot \hat{r}_{ij}\right) \tag{3.16}$$

because $\hat{r}_{ij} = -\hat{r}_{ji}$. Here, $\vec{v}_{ji} = \vec{v}_i - \vec{v}_j$; and $T_{ij} = T_i + T_j$. This T_{ij} can be interchanged to the form as shown in equation 3.9.

$$\int dT_{ij} = -\int \beta \left[2T_{ij} - v_0 \vec{v}_{ji} \cdot \hat{r}_{ij}\right] dt \implies T_{ij} + W_{ij} = C_{ij} \tag{3.17}$$

$$dW_{ij} = \beta \left[2T_{ij} - v_0 \vec{v}_{ji} \cdot \hat{r}_{ij}\right] dt \tag{3.18}$$

Here, W_{ij} is some "effective" potential for the bounded pair i, j, and C is a constant that is the consequence of the integration but this gives a criteria for the total energy. Using this, we can extract analytical criteria like we did in equation 3.10, which would help us in finding the pairs. However, we cannot analytically solve the equation 3.17 because of equation 3.18. But we can numerically integrate this.

Numerically the equations 3.16 and 3.17 can be written as:

$$\sum_k \Delta T_{ij}(t_k) + \sum_k \beta \left[2T_{ij}(t_k) - v_0(\vec{v}_i(t_k) - \vec{v}_j(t_k)) \cdot \hat{r}_{ij}\right] \Delta t = 0 \tag{3.19}$$

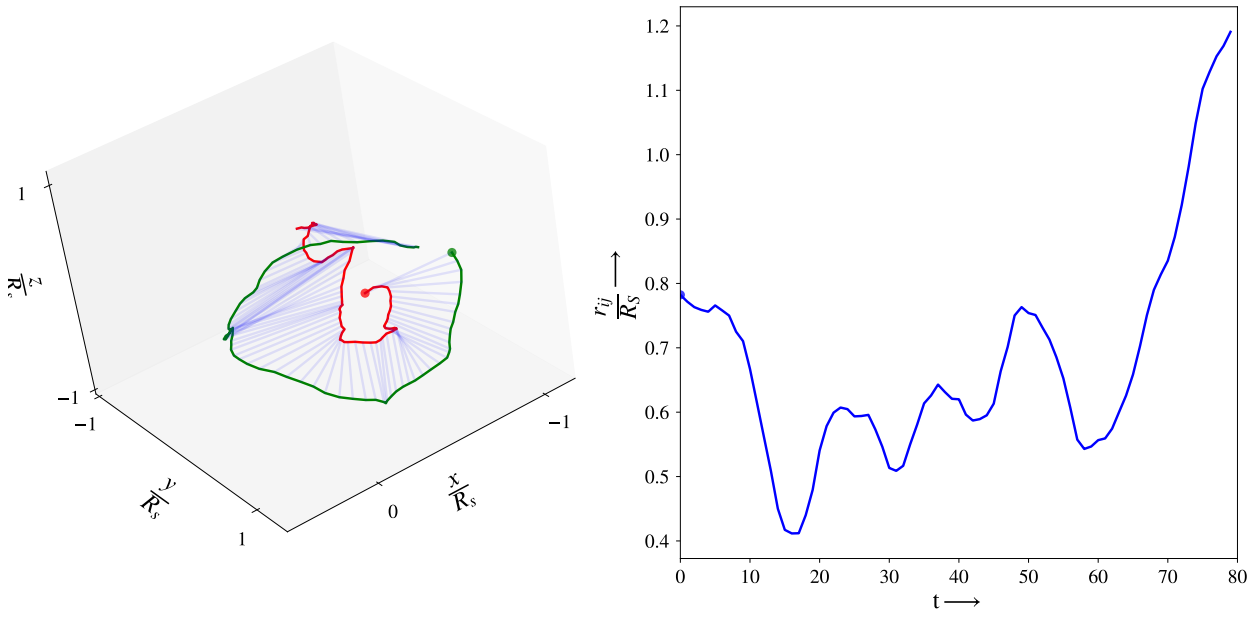

Figure 3.17: (Left) Trajectory of a pair of midges that are bounded to each other. (Right) The distance between these pairs of midges is normalized by swarm size with time. Here, $t = 0$ marks the start of pair formation. For a comparison with natural swarms, see Figure B.8.

On doing this numerical integration for many pairs, we find that the integration does not equal to zero. We speculate that this might be because we put $\hat{n}_i = \hat{r}_{ij}$. In doing so, we neglect the effects of other midges. In doing the bounded pair calculations for adaptive gravity swarms, the effect of other midges was taken into account through I_{bg} in equation 3.8. However, that didn't change the direction of the force between two bounded pairs, only its magnitude. This external effect of other midges, which changes the magnitude, can be seen in the effective potential V_{pair} in equation 3.7 through $\gamma(r_i)$, which contains I_{bg}.

Further, we are planning to add extra corrections to $\hat{n}_i \approx \hat{r}_{ij}$, to include the effect of other midges, too, to make our analysis accurate. This would appear like $\hat{n}_i \approx \delta_{\text{pair}}\hat{r}_{ij} + \delta_{\text{ext}}\hat{r}_i$.

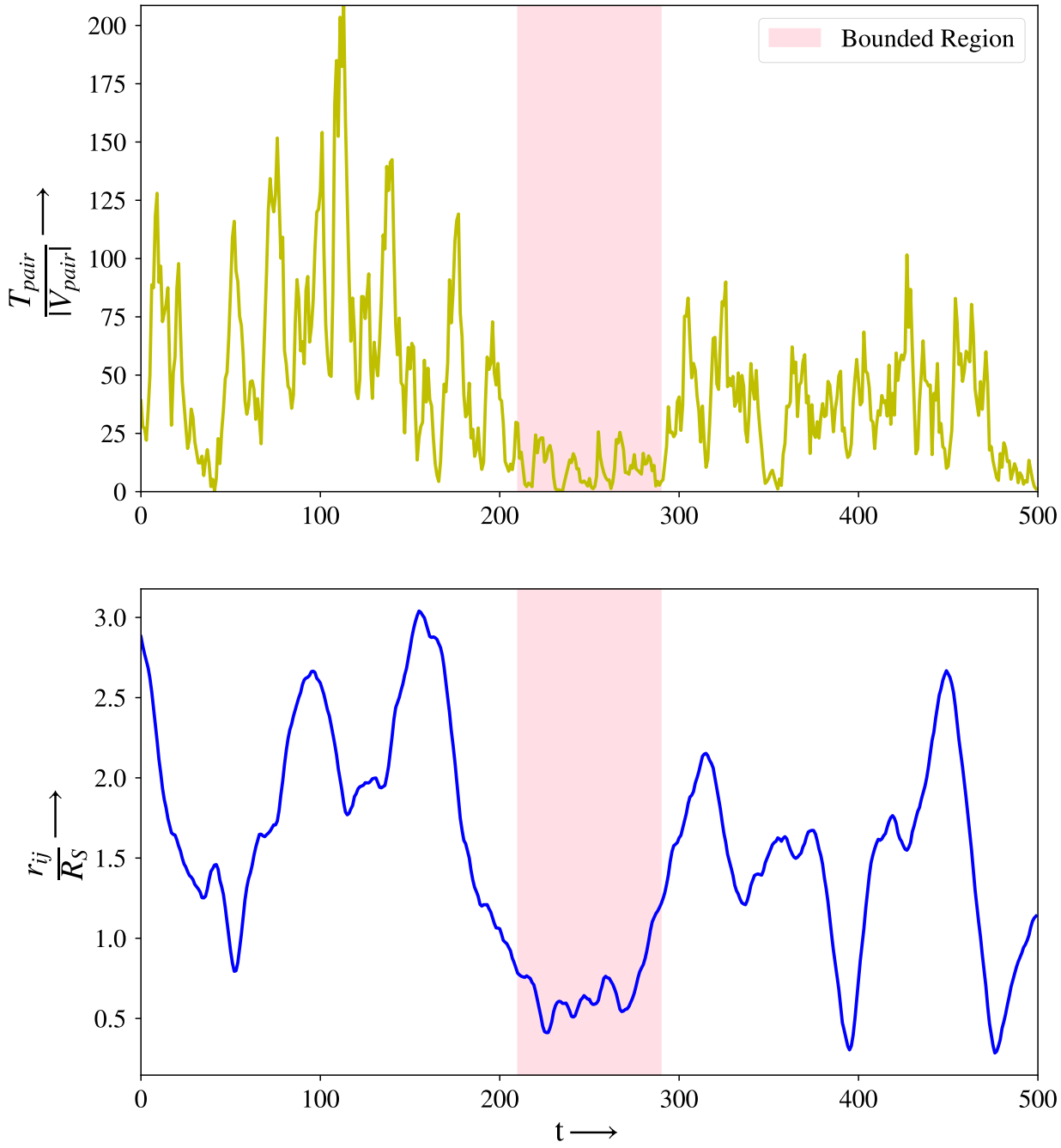

Figure 3.18: (Bottom) distance between a pair of midges normalized by swarm size. The pink region shows a bounded part of the trajectory. Note the high frequency, low amplitude behavior within the bounded part. (Top) ratio of absolute values of pair kinetic energy to pair potential energy. Note that the ratio dips during pair formation. This behavior is related to the criteria for pair formation for adaptive gravity swarms. For a comparison with natural swarms, see Figure B.8.

Chapter 4

DISCUSSION AND CONCLUSION

We have taken forward the adaptive gravity model, which already had the biological assumptions of long-range acoustic interactions and adaptivity (signal modulation), and by integrating additional assumptions of self-propulsion, heading direction, and noise. Although these new assumptions significantly transformed the mathematical equations, they could reproduce the success of the adaptive gravity model. By comparing the predictions of the adaptive gravity model for self-propelled particles with comprehensive statistical data extracted from natural insect swarms measured in the laboratory, we have successfully shown that our model is able to capture not just the cohesion of swarms but also many of their many-body dynamical characteristics. Initially, we demonstrated that our simulations generated stable swarms characterized by a constant mean size with minimal standard error of the mean. Our model reproduced the emergent harmonic oscillator behavior observed in swarming midges by showing that acceleration is proportional to the direction opposite to displacement from the center. Moreover, we presented evidence of the negative scaling of the spring constant with swarm size– a direct outcome of integrating adaptivity into gravitational interactions. Additionally, our model's acceleration and velocity statistics were qualitatively aligned with those observed in natural swarms. Furthermore, velocity kurtosis showed a similar increasing trend with swarm size; however, in our model, larger swarms displayed platykurtic characteristics, in contrast to the leptokurtic nature observed in natural swarms. Additionally, we compare the spatial distribution of velocity and acceleration, which aligned remarkably well with data from natural and adaptive gravity swarms– these could not be produced by Newtonian gravity without adaptivity. The model also successfully replicates the positive scaling between the

number of individuals and swarm size. However, natural swarms showed negative scaling with swarm size for number density, whereas our model could produce constant/weakly positive scaling. The number density values for simulated swarms are one to two orders of magnitude greater than those observed in natural swarms. Our model reproduced the Gaussian density profile of the natural swarms. An additional advantage of the model is that it provides noise as a free parameter, allowing a broader spectrum of observed dynamics. Changing the noise parameter modifies the swarm dynamics and brings the simulated swarm dynamics closer to the natural dynamics. Since the noise could be altered by insect biology, this raises the question of optimization within the natural swarms. Furthermore, our model successfully replicated pair formation, a phenomenon evident in both natural and adaptive gravity swarms, indicating it as another outcome of adaptivity in conjunction with long-range interaction. Nonetheless, the criterion for a bounded system, where the total energy equals zero, is not applicable in our scenario, necessitating the development of an appropriate metric.

As highlighted by Gorbonos et al. in their 2020 publication[17], an adaptive gravity model incorporating self-propulsion and noise is essential for accurately theorizing the midge swarm's responsiveness to external disturbances, particularly in terms of the dynamics of such reactions.

Our model, which extends the adaptive gravity framework to self-propelled particles, embodies a form of self-organized dynamics wherein the interactions among particles are sensitive to their distances. This concept is similar to the pioneering work of Cucker-Smale[21][22]. At its core, the Cucker-Smale model is a set of differential equations designed to describe how the velocity of each agent in a group converges towards a common velocity, leading to the flocking behavior observed in nature. The model assumes that each agent adjusts its velocity based on the average velocities of all other agents, weighted by a function of their mutual distances. This weighting function decreases with distance, implying that agents are more influenced by their near neighbors than those further away. However, our model differs from the Cucker-Smale (C-S) model in several important aspects. In the C-S model, velocity update (or acceleration) is inversely proportional to the total number of particles, leading to diminished effective acceleration when the particle number is large. Furthermore, the weight function within the C-S model depends on the absolute value of distance, which is in contrast to the adaptive gravity interaction that is scaled by the characteristic length

for adaptivity R_{ad}. Furthermore, the weighting function in the Cucker-Smale model is symmetric, meaning the influence exerted by particle i on particle j is equivalent to the influence of particle j on particle i. In contrast, for the adaptive gravity interaction, the influence depends on the total sound intensity experienced by particle i, rendering the weighting function asymmetric. Consequently, our adaptive gravity model for self-propelled particles serves as a more general analog to the Cucker-Smale model[23]. This model is analogous, as adaptive gravity is not an alignment interaction. Therefore, our research presents a new model for self-organized dynamics with sensitivity and non-alignment interaction.

The adaptive gravity model for self-propelled particles adeptly captures numerous properties of natural midge swarms and validates the significance of incorporating self-propulsion and noise. In biological systems, the specific interactions between the animals guiding the control of their movements are challenging to extract from experimental data. Such interactions are a product of animal communication, which encompasses a complex set of specific signals, in addition to each animal's interpretation of its counterparts' movements, intentions, and properties. Consequently, establishing a correlation between biological and active particle systems is a complex endeavor. Our active particle model, characterized by long-range interactions and adaptivity, marks remarkably well for swarming midges, underscoring its efficacy in bridging the gap between biological intricacies and theoretical modeling.

Swarming behaviors, alongside other biological phenomena, demonstrate that interactions within animal communities can manifest unique characteristics absent in physical systems, where forces typically exhibit reciprocity and are derived from potential fields. Exploring non-reciprocal interactions, inspired by the dynamics between biological entities and active systems, has become an area of increasing interest in contemporary research. In the context of swarming, such non-reciprocity comes from adaptivity. This adaptivity, coupled with long-range interactions, underpins various biological signaling mechanisms, including those mediated by light and chemical diffusion, which adhere to an inverse-square law. Consequently, this model offers a framework for simulating diverse non-reciprocal auditory, visual, and chemical communication observed in biological systems. Thus, investigating active-particle systems characterized by non-conventional

interactions promises to enhance our comprehension of animal behavior.

Appendix A

CODE LISTING

This section list the RK4 algorithm (Algorithm 1), that performs the time evolution for the molecular dynamics simulation. The DIR_NET function in the algorithm is the function mentioned in equation 2.8.

Algorithm 1 Simulation Algorithm

Noise: $\sqrt{\boldsymbol{\epsilon_x}[i,j]^2 + \boldsymbol{\epsilon_y}[i,j]^2} \leq \frac{\varepsilon}{2}$

for $t \leftarrow 0$ **to** end_time-1 **do**

$\boldsymbol{n}_{x1}[t,:], \boldsymbol{n}_{y1}[t,:] \leftarrow \text{DIR\_NET}(\boldsymbol{x}[t,:], \boldsymbol{y}[t,:])$

$\boldsymbol{a}_{x1}[t,:] \leftarrow \boldsymbol{\beta} \cdot (v_0 \cdot \boldsymbol{n}_{x1}[t,:] - \boldsymbol{v_x}[t,:]) + \boldsymbol{\epsilon_x}[t,:]$

$\boldsymbol{a}_{y1}[t,:] \leftarrow \boldsymbol{\beta} \cdot (v_0 \cdot \boldsymbol{n}_{y1}[t,:] - \boldsymbol{v_y}[t,:]) + \boldsymbol{\epsilon_y}[t,:]$

$\boldsymbol{v_x}[t,:] \leftarrow \boldsymbol{v_x}[t,:] + \boldsymbol{a}_{x1} \cdot \Delta t$

$\boldsymbol{v_y}[t,:] \leftarrow \boldsymbol{v_y}[t,:] + \boldsymbol{a}_{y1} \cdot \Delta t$

$\Delta \boldsymbol{x_1}[t,:] \leftarrow \Delta t \cdot (\boldsymbol{v_x}[t,:]$

$\Delta \boldsymbol{y_1}[t,:] \leftarrow \Delta t \cdot \boldsymbol{v_y}[t,:]$

$\boldsymbol{n}_{x2}[t,:], \boldsymbol{n}_{y2}[t,:] \leftarrow \text{DIR\_NET}(\boldsymbol{x}[t,:] + \frac{\Delta \boldsymbol{x_1}[t,:]}{2}, \boldsymbol{y}[t,:] + \frac{\Delta \boldsymbol{y_1}[t,:]}{2})$

$\boldsymbol{a}_{x2}[t,:] \leftarrow \boldsymbol{\beta} \cdot (v_0 \cdot \boldsymbol{n}_{x2}[t,:] - \boldsymbol{v_x}[t,:]) + \boldsymbol{\epsilon_x}[t,:]$

$\boldsymbol{a}_{y2}[t,:] \leftarrow \boldsymbol{\beta} \cdot (v_0 \cdot \boldsymbol{n}_{y2}[t,:] - \boldsymbol{v_y}[t,:]) + \boldsymbol{\epsilon_y}[t,:]$

$\Delta \boldsymbol{x_2}[t,:] \leftarrow \Delta t \cdot (\boldsymbol{v_x}[t,:] + \boldsymbol{a}_{x2}[t,:] \cdot \Delta t)$

$\Delta \boldsymbol{y_2}[t,:] \leftarrow \Delta t \cdot (\boldsymbol{v_y}[t,:] + \boldsymbol{a}_{y2}[t,:] \cdot \Delta t)$

$\boldsymbol{n}_{x3}[t,:], \boldsymbol{n}_{y3}[t,:] \leftarrow \text{DIR\_NET}(\boldsymbol{x}[t,:] + \frac{\Delta \boldsymbol{x_2}[t,:]}{2}, \boldsymbol{y}[t,:] + \frac{\Delta \boldsymbol{y_2}[t,:]}{2})$

$\boldsymbol{a}_{x3} \leftarrow \boldsymbol{\beta} \cdot (v_0 \cdot \boldsymbol{n}_{x3}[t,:] - \boldsymbol{v_x}[t,:]) + \boldsymbol{\epsilon_x}[t,:]$

$\boldsymbol{a}_{y3} \leftarrow \boldsymbol{\beta} \cdot (v_0 \cdot \boldsymbol{n}_{y3}[t,:] - \boldsymbol{v_y}[t,:]) + \boldsymbol{\epsilon_y}[t,:]$

$\Delta \boldsymbol{x_3}[t,:] \leftarrow \Delta t \cdot (\boldsymbol{vx}[t,:] + \boldsymbol{a}_{x3}[t,:] \cdot \Delta t)$

$\Delta \boldsymbol{y_3}[t,:] \leftarrow \Delta t \cdot (\boldsymbol{vy}[t,:] + \boldsymbol{a}_{y3}[t,:] \cdot \Delta t)$

$\boldsymbol{n}_{x4}[t,:], \boldsymbol{n}_{y4}[t,:] \leftarrow \text{DIR\_NET}(\boldsymbol{x}[t,:] + \Delta \boldsymbol{x_3}[t,:], \boldsymbol{y}[t,:] + \Delta \boldsymbol{y_3}[t,:])$

$\boldsymbol{a}_{x4}[t,:] \leftarrow \boldsymbol{\beta} \cdot (v_0 \cdot \boldsymbol{n}_{x4}[t,:] - \boldsymbol{v_x}[t,:]) + \boldsymbol{\epsilon_x}[t,:]$

$\boldsymbol{a}_{y4}[t,:] \leftarrow \boldsymbol{\beta} \cdot (v_0 \cdot \boldsymbol{n}_{y4}[t,:] - \boldsymbol{v_y}[t,:]) + \boldsymbol{\epsilon_y}[t,:]$

$\Delta \boldsymbol{x_4}[t,:] \leftarrow \Delta t \cdot (\boldsymbol{v_x}[t,:] + \boldsymbol{a}_{x4}[t,:] \cdot \Delta t)$

$\Delta \boldsymbol{y_4}[t,:] \leftarrow \Delta t \cdot (\boldsymbol{v_y}[t,:] + \boldsymbol{a}_{y4}[t,:] \cdot \Delta t)$

$$\boldsymbol{x}[t+1,:] \leftarrow \boldsymbol{x}[t,:] + \frac{\Delta \boldsymbol{x_1}[t,:] + 2 \cdot \Delta \boldsymbol{x_2}[t,:] + 2 \cdot \Delta \boldsymbol{x_3}[t,:] + \Delta \boldsymbol{x_4}[t,:]}{6}$$

$$\boldsymbol{y}[t+1,:] \leftarrow \boldsymbol{y}[t,:] + \frac{\Delta \boldsymbol{y_1}[t,:] + 2 \cdot \Delta \boldsymbol{y_2}[t,:] + 2 \cdot \Delta \boldsymbol{y_3}[t,:] + \Delta \boldsymbol{y_4}[t,:]}{6}$$

$$\boldsymbol{v_x}[t+1,:] \leftarrow \frac{\boldsymbol{x}[t+1,:] - \boldsymbol{x}[t,:]}{\Delta t}$$

$$\boldsymbol{v_y}[t+1,:] \leftarrow \frac{\boldsymbol{y}[t+1,:] - \boldsymbol{y}[t,:]}{\Delta t}$$

Appendix B

Natural and Adaptive Gravity Swarms

This sections consists of plots for natural swarms and adaptive gravity swarms from previous papers[4][16][17][18].

- Figure B.1, B.2 are from [4].
- Figure B.3, B.4, B.5, B.6, B.7 are from [17].
- Figure B.8 are from [18].

These plots are for comparison against the results produced by our adaptive gravity for self-propelled particles simulations presented in chapter 3.

- Simulated figures Figure 3.4, 3.6, 3.8 are compared against empirical figures Figure B.1.
- Simulated figures Figure 3.7 are compared against empirical figures Figure B.2.
- Simulated figures Figure 3.9 are compared against empirical figures Figure B.3, B.4.
- Simulated figures Figure 3.10 are compared against empirical figures Figure B.5.
- Simulated figures Figure 3.11 are compared against empirical figures Figure B.6.
- Simulated figures Figure 3.12 are compared against empirical figures Figure B.7.
- Simulated figures Figure 3.17, 3.18 are compared against empirical figures Figure B.8.

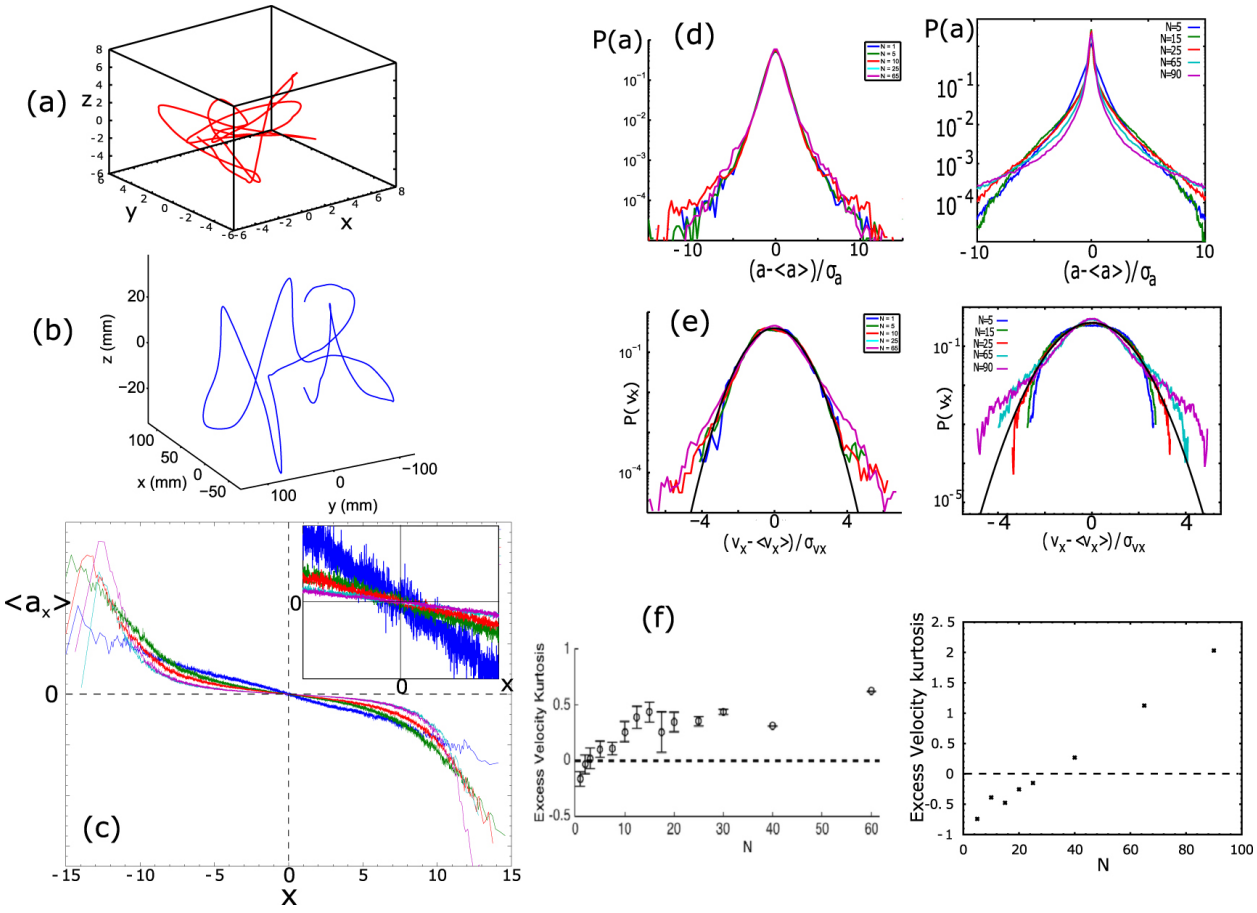

Figure B.1: Comparison of the adaptive-gravity simulations to experimental observations. (a) A sample simulated trajectory from a swarm of $N = 50$ midges, as compared with (b) an observed trajectory in a swarm of $N = 25$ midges. (c) Simulated mean acceleration along the x-axis as a function of position for swarms of various sizes ($N = 15, 25, 40, 90$, from top to bottom). The top right inset shows the simulated linear behavior near the swarm center, and the dependence of the slope on the swarm size (different colors). (d) Observed acceleration distribution (left panel), compared to the simulation results (right panel). Both display highly non-Gaussian tails. (e) Observed x-component velocity distribution (left panel), compared to the simulation results (right panel). Both show that small swarms have a roughly Gaussian velocity distribution, but large swarms develop heavy tails. This tendency is quantified in f, where the excess kurtosis is plotted as a function of swarm size, and both observations (left panel) and simulations (right panel) indicate a negative excess kurtosis for small swarms and a positive kurtosis (due to the roughly exponential tails in the distributions) for large swarms.

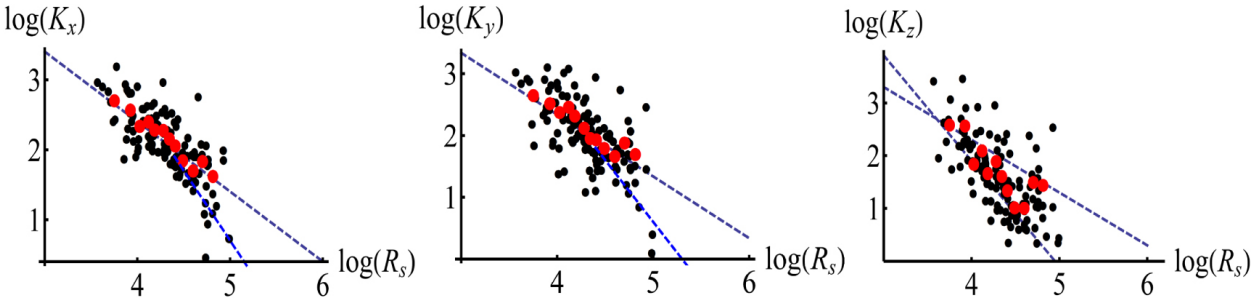

Figure B.2: Effective spring constants in the horizontal directions (K_x and K_y) and the vertical direction (K_z) as a function of the average swarm radius R_S, plotted on logarithmic axes. The black circles denote the raw data for each swarm, the red circles show binned averages, and the dashed lines denote the R_S^{-1} scaling predicted by the adaptive gravity model. We also plot the R_S^{-2} scaling predicted for cylindrical swarms, which seems to fit the behavior of larger swarms. Note that in the vertical z-direction the data is more scattered, which may be due to Earth's gravity.

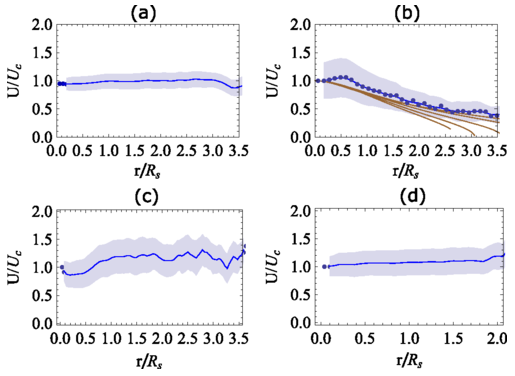

Figure B.3: Mean speed as a function distance from the center of the swarm, normalized by the speed at the center. Data are shown for (a) real laboratory swarms, (b) epsilon-gravity, (c) adaptive gravity, and (d) adaptive gravity with short-range repulsion. The brown curves in (b) correspond to a family of King model solutions. In (d), we truncated the plot at $r \sim 2R_S$ since outside this radius the particles are not part of the cohesive region (i.e., the swarm).

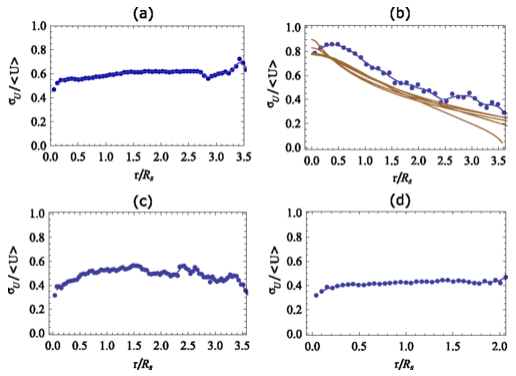

Figure B.4: The standard deviation of the speed (σ_U) normalized by the average speed in the swarm as a function of the distance from the center of mass normalized by the swarm size R_S. Data are shown for (a) laboratory observations, (b) simulation of ε-gravity [note that the brown curves correspond to a family of King solutions computed numerically], (c) adaptive gravity, and (d) adaptive gravity with repulsion.

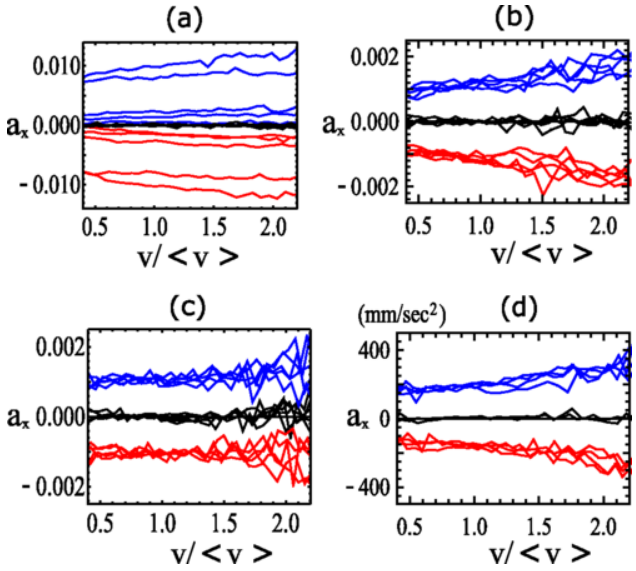

Figure B.5: The mean value of a single component of the acceleration versus the speed (normalized by the average speed) of the left hemisphere (blue), right hemisphere (red), and both hemispheres (black). The overall acceleration (black lines) is close to zero, as required by symmetry. Data are shown for (a) ε-gravity for different values of R_S (with $R_S = 16.23, 3.16, 19.53, 18.37, 30.10$ from top to bottom), (b) adaptive gravity, (c) adaptive gravity with repulsion, and (d) natural swarms.

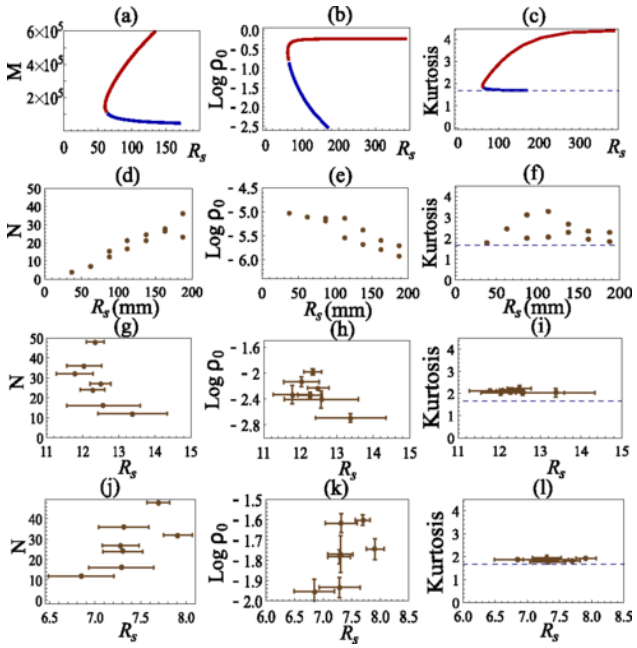

Figure B.6: (a)–(c) Total mass M (a), density at the center ρ_0 (b), and kurtosis (c) as a function of the swarm size R_S for a series of King model solutions. The blue line corresponds to the stable branch in the canonical ensemble and the red one to the unstable one. The kurtosis of a Gaussian distribution in three dimensions, $5/3$, is denoted by the horizontal dashed line. (d)–(f) The same quantities computed from the measured data for real swarms. (g)–(i) The same quantities computed for simulated swarms with adaptivity. (j)–(l) The same quantities computed for simulated swarms with adaptivity and short-range repulsion.

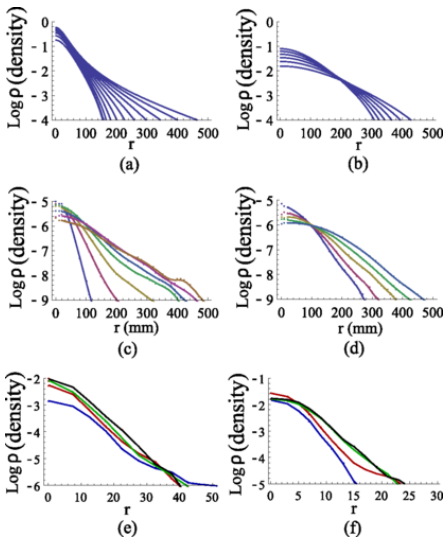

Figure B.7: (a), (b) Two families of density profiles computed from the King model for different initial conditions, with shapes that are qualitatively similar to results from real swarms (c), (d). (a) corresponds to the unstable branch and (b) to the stable branch. (c), (d) Two families of density profiles measured in real swarms in two different laboratory setups (see text). (e) Density profiles of simulated swarms using the adaptive gravity model. Simulations were run using $N = 12$ and $R_S = 16.2$ (blue), $N = 24$ and $R_S = 11.8$ (red), $N = 32$ and $R_S = 11.5$ (green), and $N = 48$ and $R_S = 12$ (black). (f) Density profiles of simulated swarms including adaptivity and short-range repulsion. Simulations were run using $N = 12$ and $R_S = 6$ (blue), $N = 24$ and $R_S = 6.7$ (red), $N = 32$ and $R_S = 8.2$ (green), and $N = 48$ and $R_S = 8.1$ (black).

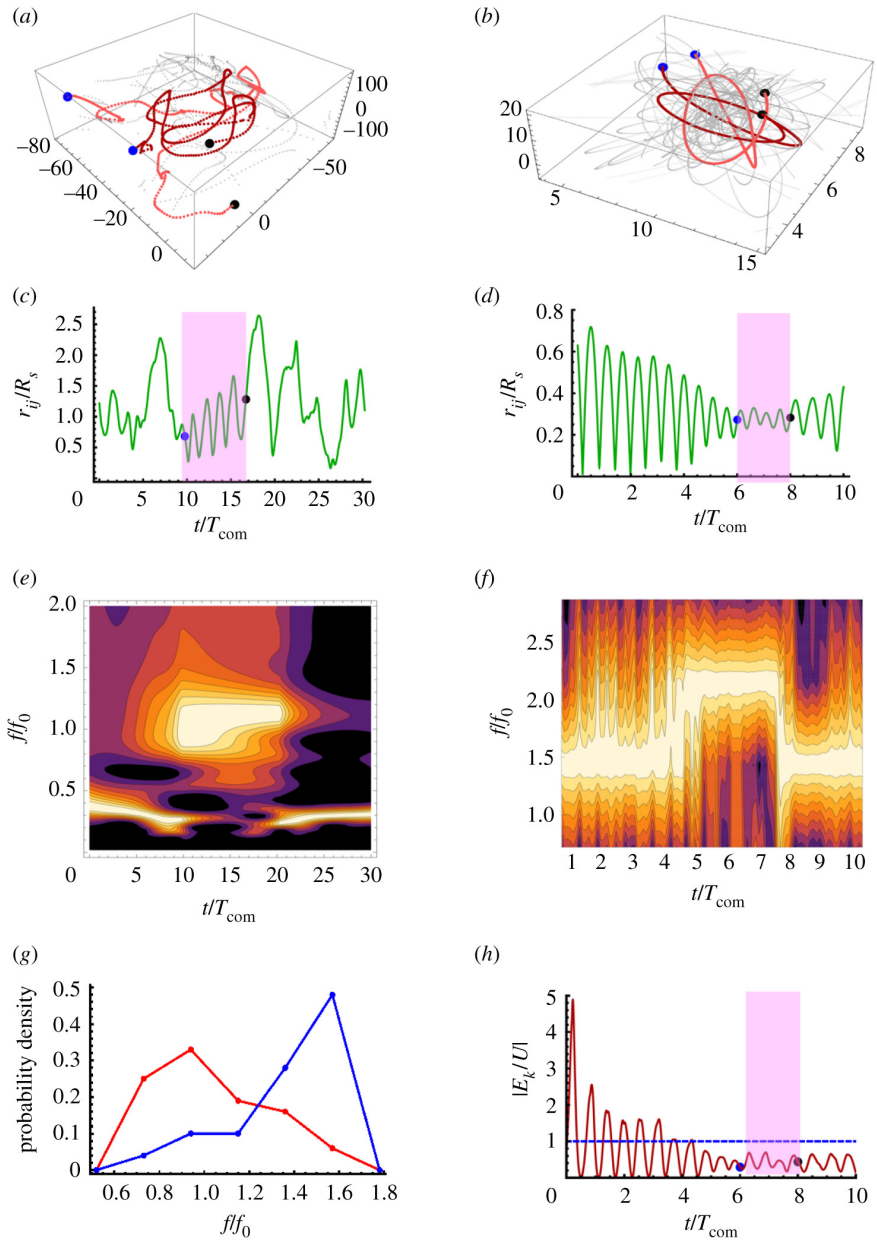

Figure B.8: Pairs in laboratory observations of midge swarms (a,c,e) and simulations of the adaptive gravity model (b,d,f). (a) Trajectories of two midges in a laboratory swarm that exhibited pairing (defined in the section 3.4). The midges were identified as belonging to a pair between the blue and black points. Paired parts of the trajectories are coloured in red, while unpaired parts are in grey. Distances are in millimetres. (b) A pair as identified in a simulation of the adaptive gravity. Symbols and colours are the same as in (a). Distances are in simulation unit lengths. Note that the simulated pair is defined by the energy ratio given in (h), but we plot here just the duration marked in (h) for clarity. (c,d) Distance between the members of the laboratory pair (c) and simulated pair (d) as a function of time. The blue and the black points correspond to the beginning and end of the red trajectories (a,b). The distance is normalized by the swarm size R_S, which is defined as the mean distance of a midge from the centre of mass of the swarm. Time is normalized by the typical orbit time around the centre of mass, defined as $T_{com} = 4R_S/\bar{v}$, where $\bar{v}$ is the mean midge speed. In the laboratory observations, R_S is typically on the order of 100 mm and $\bar{v}$ is roughly 100 mm s^{-1}. In the example here the laboratory swarm consists of $N = 21$ midges. The simulated swarm has $N = 30$, $R_{ad} = 15$, $R_S = 5.08$ and $\bar{v} = 0.028$. (e) Time-frequency analysis of the motion of the laboratory pair using a continuous wavelet transform. Frequencies are normalized by the typical frequency $f_0 = 1/T_{com}$ and the amplitude by the time-resolved peak power $F_{max}(t)$. Higher powers are represented with brighter colours. During pairing, the peak power shifts to higher frequencies. (f) Time-frequency analysis of the motion of the simulated pair using a windowed Fourier transform with a window length of $0.14T_{com}$. The behaviour is similar to what is seen in the laboratory pair. (g) Probability density function of the peak frequency of motion in the simulation during pairing (blue) and independent motion (red). (h) The ratio of kinetic to potential energy for the example shown in (b).

BIBLIOGRAPHY

[1] M. Ballerini, N. Cabibbo, R. Candelier, *et al.*, "Interaction ruling animal collective behavior depends on topological rather than metric distance: Evidence from a field study," en, *Proceedings of the National Academy of Sciences*, vol. 105, no. 4, pp. 1232–1237, Jan. 2008, ISSN: 0027-8424, 1091-6490. DOI: 10.1073/pnas.0711437105.

[2] J. Krause and G. D. Ruxton, *Living in groups* (Oxford series in ecology and evolution). Oxford ; New York: Oxford University Press, 2002, OCLC: ocm48532770, ISBN: 978-0-19-850817-5 978-0-19-850818-2.

[3] R. T. Sullivan, "Insect Swarming and Mating," *The Florida Entomologist*, vol. 64, no. 1, p. 44, Mar. 1981, ISSN: 00154040. DOI: 10.2307/3494600.

[4] D. Gorbonos, R. Ianconescu, J. G. Puckett, R. Ni, N. T. Ouellette, and N. S. Gov, "Long-range acoustic interactions in insect swarms: An adaptive gravity model," *New Journal of Physics*, vol. 18, no. 7, p. 073 042, Jul. 2016, ISSN: 1367-2630. DOI: 10.1088/1367-2630/18/7/073042.

[5] J. G. Puckett, D. H. Kelley, and N. T. Ouellette, "Searching for effective forces in laboratory insect swarms," en, *Scientific Reports*, vol. 4, no. 1, p. 4766, Apr. 2014, ISSN: 2045-2322. DOI: 10.1038/srep04766.

[6] J. G. Puckett and N. T. Ouellette, "Determining asymptotically large population sizes in insect swarms," en, *Journal of The Royal Society Interface*, vol. 11, no. 99, p. 20 140 710, Oct. 2014, ISSN: 1742-5689, 1742-5662. DOI: 10.1098/rsif.2014.0710.

[7] A. Attanasi, A. Cavagna, L. Del Castello, *et al.*, "Collective Behaviour without Collective Order in Wild Swarms of Midges," en, *PLoS Computational Biology*, vol. 10, no. 7, T. Vicsek, Ed., e1003697, Jul. 2014, ISSN: 1553-7358. DOI: 10.1371/journal.pcbi.1003697.

[8] R. Ni and N. Ouellette, "Velocity correlations in laboratory insect swarms," en, *The European Physical Journal Special Topics*, vol. 224, no. 17-18, pp. 3271–3277, Dec. 2015, ISSN: 1951-6355, 1951-6401. DOI: 10.1140/epjst/e2015-50077-5.

[9] M. Bär, R. Großmann, S. Heidenreich, and F. Peruani, "Self-Propelled Rods: Insights and Perspectives for Active Matter," en, *Annual Review of Condensed Matter Physics*, vol. 11, no. 1, pp. 441–466, Mar. 2020, ISSN: 1947-5454, 1947-5462. DOI: 10.1146/annurev-conmatphys-031119-050611. URL: https://www.annualreviews.org/doi/10.1146/annurev-conmatphys-031119-050611 (visited on 03/16/2024).

[10] N. T. Ouellette, "A physics perspective on collective animal behavior," eng, *Physical biology*, vol. 19, no. 2, pp. 21 004–, 2022, Publisher: IOP Publishing, ISSN: 1478-3975. DOI: 10.1088/1478-3975/ac4bef.

[11] T. Vicsek and A. Zafeiris, "Collective motion," en, *Physics Reports*, vol. 517, no. 3-4, pp. 71–140, Aug. 2012, ISSN: 03701573. DOI: 10.1016/j.physrep.2012.03.004.

[12] D. Sumpter, "The principles of collective animal behaviour," en, *Philosophical Transactions of the Royal Society B: Biological Sciences*, vol. 361, no. 1465, pp. 5–22, Jan. 2006, ISSN: 0962-8436, 1471-2970. DOI: 10.1098/rstb.2005.1733.

[13] I. Giardina, "Collective behavior in animal groups: Theoretical models and empirical studies," en, *HFSP Journal*, vol. 2, no. 4, pp. 205–219, Aug. 2008, ISSN: 1955-2068. DOI: 10.2976/1.2961038.

[14] M. Brambilla, E. Ferrante, M. Birattari, and M. Dorigo, "Swarm robotics: A review from the swarm engineering perspective," en, *Swarm Intelligence*, vol. 7, no. 1, pp. 1–41, Mar. 2013, ISSN: 1935-3812, 1935-3820. DOI: 10.1007/s11721-012-0075-2.

[15] N. T. Ouellette, "Empirical questions for collective-behaviour modelling," en, *Pramana*, vol. 84, no. 3, pp. 353–363, Mar. 2015, ISSN: 0304-4289, 0973-7111. DOI: 10.1007/s12043-015-0936-5.

[16] D. Gorbonos and N. S. Gov, "Stable swarming using adaptive long-range interactions," en, *Physical Review E*, vol. 95, no. 4, p. 042 405, Apr. 2017, ISSN: 2470-0045, 2470-0053. DOI: 10.1103/PhysRevE.95.042405.

[17] D. Gorbonos, K. Van Der Vaart, M. Sinhuber, J. G. Puckett, A. M. Reynolds, N. T. Ouellette, and N. S. Gov, "Similarities between insect swarms and isothermal globular clusters," en, *Physical Review Research*, vol. 2, no. 1, p. 013 271, Mar. 2020, ISSN: 2643-1564. DOI: 10.1103/PhysRevResearch.2.013271.

[18] D. Gorbonos, J. G. Puckett, K. Van Der Vaart, M. Sinhuber, N. T. Ouellette, and N. S. Gov, "Pair formation in insect swarms driven by adaptive long-range interactions," en, *Journal of The Royal Society Interface*, vol. 17, no. 171, p. 20 200 367, Oct. 2020, ISSN: 1742-5689, 1742-5662. DOI: 10.1098/rsif.2020.0367.

[19] M. Adler and U. Alon, "Fold-change detection in biological systems," en, *Current Opinion in Systems Biology*, vol. 8, pp. 81–89, Apr. 2018, ISSN: 24523100. DOI: 10.1016/j.coisb.2017.12.005.

[20] J. G. Puckett, R. Ni, and N. T. Ouellette, "Time-Frequency Analysis Reveals Pairwise Interactions in Insect Swarms," en, *Physical Review Letters*, vol. 114, no. 25, p. 258 103, Jun. 2015, ISSN: 0031-9007, 1079-7114. DOI: 10.1103/PhysRevLett.114.258103.

[21] F. Cucker and S. Smale, "Emergent Behavior in Flocks," *IEEE Transactions on Automatic Control*, vol. 52, no. 5, pp. 852–862, May 2007, ISSN: 0018-9286. DOI: 10.1109/TAC.2007.895842.

[22] F. Cucker and S. Smale, "On the mathematics of emergence," en, *Japanese Journal of Mathematics*, vol. 2, no. 1, pp. 197–227, Mar. 2007, ISSN: 0289-2316, 1861-3624. DOI: 10.1007/s11537-007-0647-x.

[23] S. Motsch and E. Tadmor, "A New Model for Self-organized Dynamics and Its Flocking Behavior," en, *Journal of Statistical Physics*, vol. 144, no. 5, pp. 923–947, Sep. 2011, ISSN: 0022-4715, 1572-9613. DOI: 10.1007/s10955-011-0285-9.